Present-day development of gully-channel sinuosity by carbon dioxide gas supported flows on Mars

Kelly Pasquon, Julien Gargani, Marion Massé, Mathieu Vincendon, Susan J. Conway, Antoine Séjourné, Vincent Jomelli, Matthew Balme, Simon Lopez, Anthony Guimpier

Present-day development of gully-channel sinuosity by carbon dioxide gas supported flows on Mars

Kelly Pasquon[a b*]; Julien Gargani[ac]; Marion Massé[d]; Mathieu Vincendon[e] ; Susan J. Conway[d]; Antoine Séjourné[a], Vincent Jomelli[f], Matthew R. Balme[g], Simon Lopez[h], Anthony Guimpier[d]

[a] GEOPS, Univ. Paris-Sud, CNRS, University Paris-Saclay, rue du Belvédère, Bât. 504-509, 91405 Orsay, France
kelly.pasquon@u-psud.fr, julien.gargani@u-psud.fr, antoine.sejourne@u-psud.fr

[b] Cerema Ouest, Maison de l'Administration Nouvelle, 9 Rue René Viviani, 44200 Nantes, France
kelly.pasquon@cerema.fr

[c] Centre d'Alembert, Univ. Paris-Sud, University Paris-Saclay rue du Doyen Georges Poitou, Bât 407, 91405 Orsay, France

[d] LPG, Univ. Nantes UMR-CNRS 6112, 2 rue de la Houssinière, 44322 Nantes, France
marion.masse@univ-nantes.fr, susan.conway@univ-nantes.fr

[e] IAS, Univ. Paris-Sud, CNRS, University Paris-Saclay, rue Jean-Dominique Cassini, 91440 Bures-sur-Yvette
mathieu.vincendon@u-psud.fr

[f] LGP, CNRS, Univ. Paris 1-4, 1 Place Aristide Briand, 92195 Meudon, France
Vincent.JOMELLI@lgp.cnrs.fr

[g] Planetary Environments Group, Open University, Walton Hall, Milton Keynes, UK
matt.balme@open.ac.uk

[h] BRGM, 3 avenue Claude Guillemin, 45000 Orléans, France
s.lopez@brgm.fr

*corresponding author

Martian gullies have been widely studied, but their formation mechanism is still under debate. Their channels generally trend straight downslope, but some display

sinuosity. Seasonally active gullies are common on sand dunes and their channels have been reported to develop sinuosity. Here, we perform a detailed analysis of a gully on a dune within Matara Crater (49.5°S; 34.9°E) where development of channel sinuosity has taken place over 5 martian years (MY29-33) of observation. This study was performed using HiRISE images, HiRISE elevation data, spectroscopic CRISM data and a 1D GCM for surface temperature modelling. The morphological evolution of the gully suggests a significant seasonal contribution of fluid. Each year we observed material collapse and accumulation in the alcove, followed by transport events during which lateral migration and extension of the channel occur together with growth of the debris apron. Over one martian year, the debris apron propagated by almost 140 meters from an initial length of 800 meters. These transport events occur in the middle of winter when CO_2 frost is still present and are contemporaneous with the beginning of the defrosting. We propose that the activity and the sinuosity development in the gully could be explained by: 1) a flow composed of sand and CO_2 gas, producing morphologies similar to those in hyper-concentrated flows on Earth and 2) contribution of material from alternating of the alcove source location.

Keywords: Mars; Mars surface; Mars climate; Geological processes; Ices.

1 Introduction

1.1 Context and objective

Since their first observation by Malin and Edgett (2000), martian gullies have been abundantly studied (e.g., Harrison et al., 2015). Despite this profusion of research, no clear consensus on their formation mechanism has been reached. The two main hypotheses for the formation of martian gullies involve either melting of water ice or sublimation of CO_2 ice (e.g., Conway et al., 2018). The difficulty in converging toward a unique interpretation may be related to the significant variability in morphologies (Auld and Dixon, 2016) associated with the term “gully”, as this variability may indicate that various processes form or modify gullies.

Gullies are generally composed of an alcove, a channel and an apron (Malin and Edgett, 2000; Harrison et al., 2015), and in some cases the channel can be highly sinuous (e.g., Mangold et al., 2010; Pasquon et al., 2016; Dundas et al., 2017). Active modification of gullies has been recently observed on Mars (Reiss and Jaumann, 2003; Reiss et al., 2010; Diniega et al., 2010; 2013; Hansen et al., 2011;

Dundas et al., 2010; 2012; 2015; 2017; Raack et al., 2015; Jouannic et al., 2012; Pasquon et al., 2016, 2018), including reports of the development of channel sinuosity (Dundas et al., 2017). The timing of this present-day activity is generally constrained to the autumn to early spring when CO_2 ice is present on the surface. Although Vincendon (2015) found that only H_2O ice was present during some of the reported activity and Pasquon et al. (2016) found that linear gullies on sand dunes are only active as the last CO_2 frost is removed, conditions cited as particularly favorable for water ice melt (Kossacki and Markiewicz, 2004).

Here we perform detailed analysis of the development and migration of a sinuous channel observed over 5 martian years (MY29-33) of a gully located on the dunefield of Matara Crater (49.5°S; 34.9°E). The aim of this study is to better understand the processes leading to the development of channel sinuosity and the role of volatiles H_2O and CO_2 in developing this morphology.

1.2 Martian gullies

Gullies on Mars are common and are mainly located between 30° and 50°N/S. They are particularly abundant in the southern hemisphere (e.g., Balme et al., 2006; Dickson et al., 2007; Harrison et al., 2015; Dundas et al., 2015). Most gullies are observed on crater walls, central peaks, valley walls and mesas (e.g., Malin and Edgett, 2000; Dundas et al., 2010; 2012; 2015; Harrison et al., 2015; Raack et al., 2015), but gullies are also found entirely within superficial sediments, such as on sand dunes (e.g., Diniega et al., 2010; Hansen et al., 2011; Dundas et al., 2012; Jouannic et al., 2012; 2018; Pasquon et al., 2016; 2018). Gullies originating at bedrock surfaces, such as crater walls, are far more common than gullies on sand dunes, which form ~0.6% of all gullies (Conway et al., 2018), yet 35% of active gullies are on sand dunes (Dundas et al., 2015). Multiple processes have been proposed to explain the formation of gullies including: liquid water from ground water aquifers (Malin and Edgett, 2000; Mellon and Phillips, 2001; Heldmann and Mellon, 2004; Heldmann et al., 2005; Malin et al., 2006), geothermal activity (Gaidos, 2001; Hartmann, 2001), melting of shallow ground ice (Costard et al., 2002; Reiss and Jaumann, 2003; Mangold et al., 2003; 2010; Miyamoto et al., 2004; Balme et al., 2006; Reiss et al., 2010; Conway et al., 2011; Jouannic et al., 2012; 2015; Conway and Balme, 2016), snowmelt (Lee et al., 2001; Christensen, 2003; Dickson et al., 2007; Védie et al., 2008; Hauber et al., 2011; Williams et al., 2009), frosted granular

flow (Hugenholtz, 2008), CO_2-supported debris flows or blocks (Hoffman, 2002; Ishii and Sasaki, 2004; Di Achille et al., 2008; Diniega et al., 2010; Cedillo-Flores et al., 2011; Dundas et al., 2012; 2017; Pilorget and Forget, 2015), release of liquid CO_2 (Musselwhite et al., 2001), dry mass wasting (Treiman, 2003; Shinbrot et al., 2004), and the presence of brines (Knauth and Burt, 2002; Ojha et al., 2015; Massé et al., 2016).

Some gullies are still active today and the timing of their activity suggests that they are triggered by seasonal processes (e.g., Dundas et al., 2010; Pasquon et al., 2016). Seasonal processes have been generally attributed to the defrosting of CO_2 (e.g., Dundas et al., 2012; 2015; 2017). CO_2 is omnipresent on Mars: when the temperature decreases in winter, deposits of solid CO_2 and a small quantity of water ice can accumulate at the surface from direct condensation of the atmosphere in contact with the cold surface or through precipitation of ice crystals from the cold atmosphere. During winter, such deposits i) cover all surfaces above ~60° latitude, ii) are discontinuous from 40° to 60° latitude (Schorghofer and Edgett, 2006; Vincendon et al., 2010b; Diniega et al., 2013), and iii) are limited to pole-facing slopes nearer the equator (Vincendon et al., 2010b; Dundas et al., 2015; 2017). These deposits can be up to meters in thickness near the poles (Smith et al., 2001), but are generally sub-centimeter thickness at lower latitudes (Vincendon, 2015). Most of this frost is composed of CO_2 that can reach a few centimeters in thickness (Diniega et al., 2013; Dundas et al., 2015), and H_2O is a minor component estimated to be of the order of micrometers in thickness (Kereszturi et al., 2009; Gardin et al., 2010; Vincendon et al., 2010b).

An impermeable layer of ground ice under a thin layer of dry regolith is thought to exist on Mars (e.g., Mellon et al. 2004; Vincendon et al., 2010a; Jouannic et al., 2015; Dundas et al., 2018). It is also hypothesized to be present within dunes (e.g., Fenton and Hayward 2010). Two indications point to this: i) material is transported over kilometers during gully activity indicates limited infiltration and a thin active layer, ii) the CO_2 ice sublimates earlier than predicted because the ice within the dunes increases their thermal inertia (Vincendon et al., 2010b; Jouannic et al., 2012).

1.3 Sinuous gullies

Gullies are generally composed of an alcove, a channel and a debris apron, but many different types of gullies exist: those without an apron; those with numerous

alcoves contributing to a single channel, those with a relatively small debris apron, those with no tributaries, those with many tributaries, or those with or without lateral levees, etc… Auld and Dixon (2016) defined seven morphological classes of gullies and all of these classes can have channel sinuosity. The sinuosity of a channel is determined by the sinuosity index "S", which is the ratio between the total channel length (L1) and the straight line from the top to the bottom of the channel (L0). For a channel to be classed as sinuous it must have a sinuosity index, $S > 1.05$ (Mangold et al., 2010). On Mars, gullies with sinuous channels are located adjacent to gullies without sinuous channels, hence are found in both hemispheres of Mars and more frequently between 30° and 50° in latitude (Malin and Edgett, 2000; Balme et al., 2006). These sinuous gullies occur over a large range of elevations (Mangold et al., 2010). However, they do not often occur at low elevation (Mangold et al., 2010). Channels generally have widths of up to a few meters (Mellon and Phillips, 2001) and lengths up to a few kilometers (Heldmann and Mellon, 2004). They often become narrower and shallower downslope (Mangold et al., 2010). Sinuous channel occur on slopes between 10° and 20°, but most precisely between 12° and 14° (Mangold et al., 2010). Their preferential orientation is pole-facing slopes (Mangold et al., 2010) similar to the general population (e.g., Conway et al. 2017).

Two different types of channel sinuosity are visible in gullies on Mars: 1) sinuosity of channels expressed between symmetric lateral levees (Fig. 1A) usually found in "linear" dune gullies, 2) sinuosity developed with both in-channel erosion and deposition (see Edwards and Liverpool, 1995) (Fig. 1B).

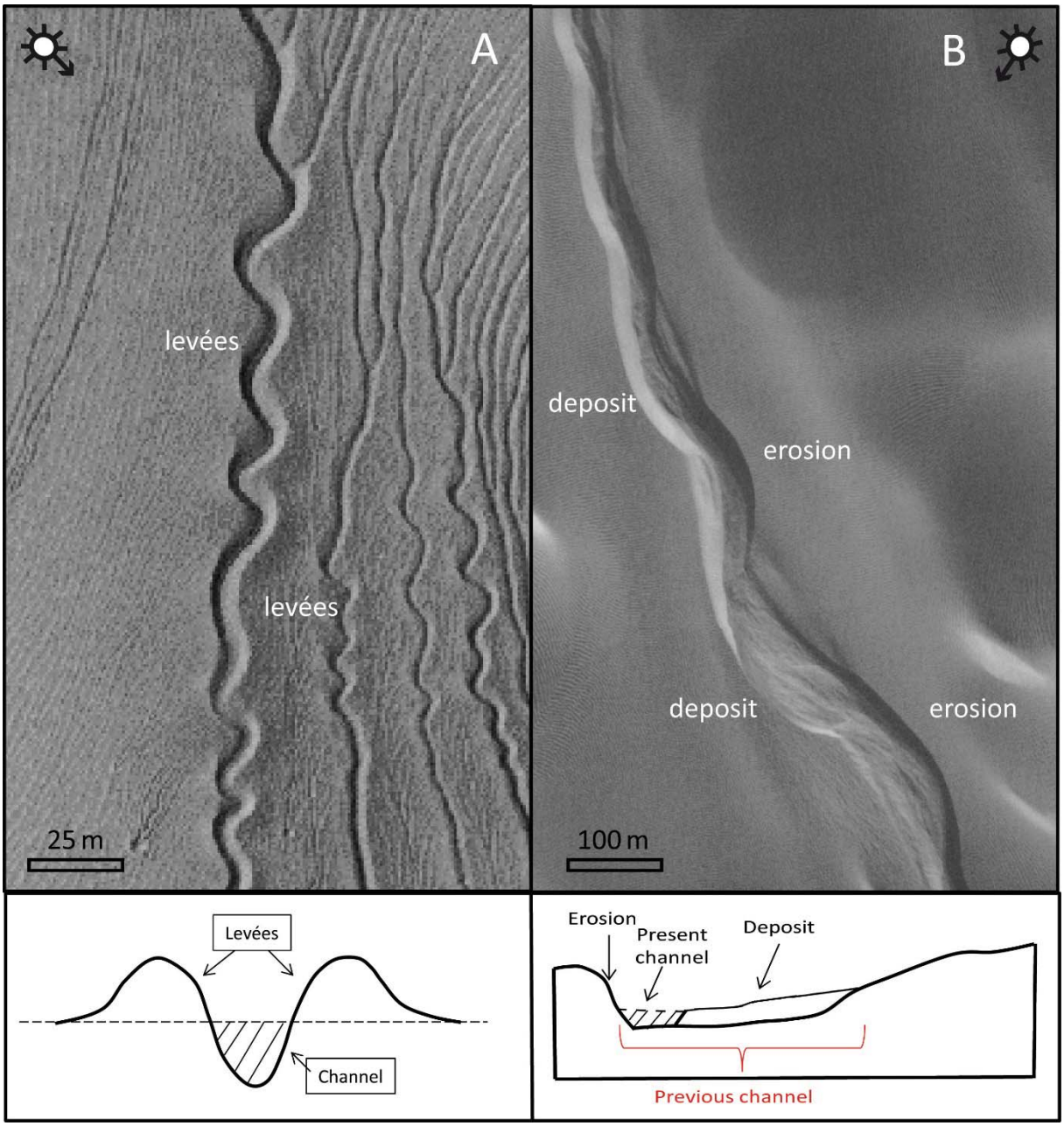

Fig. 1. A) Example of sinuous gully channels with levees on Mars. B) Example of a sinuous gully channel without lateral levees and with areas of erosion as well as sedimentation in the channel.

The first type of sinuosity is thought to be caused by debris flow processes and the second could be due to hyper-concentrated flow (Mangold et al., 2010). Debris flows are composed of a mix of liquid water and solid material ranging between 20 and 60% with a grain size ranging from micrometers to meters scale (e.g., Allen, 1985; Coussot and Meunier, 1996). Debris flows can be generalized as viscous flows, with a viscosity ranging from 1 to 10000 Pa.s, which can transport boulders several meters in size. They can propagate over slopes <10° and even down to 1 to 2° on Earth. Hyper-concentrated flows are liquid water flows, which typically contain more

than 30% of solid material. Hyper-concentrated flows can have an intermediate state between turbulent stream flows and laminar viscous debris flows (e.g., Allen, 1997). Mangold et al. (2010) concluded that sinuous gully channels are formed by the same processes as straight ones. The present-day initiation and migration of sinuous channels have been reported by Dundas et al., (2015; 2017): on crater walls at 37.5°S; 222.9°E and at 38.9°S; 196°E and on dunes at 47.6°S; 30.4°E and at 49.5°S; 34.9°E. These morphologies are interpreted to be driven by processes related to the seasonal CO_2 frost (Dundas et al., 2015; 2017). Dundas et al. (2017) report that sinuous channels were observed to migrate and become more sinuous. Cutoff of a channel bend was also reported, analogous to the formation of an oxbow lake in a meandering stream (Dundas et al., 2017). Dundas et al. (2017) suggest that energetic flows are required to create such sinuous channels. Linear dune gullies have been described as being formed by debris flow processes (Mangold et al., 2003; Jouannic et al., 2012). Recently linear dune gullies have been shown to be an active seasonal phenomena (Diniega et al., 2013; Pasquon et al., 2016; Jouannic et al. 2018). Linear dune gullies, despite their name, can have a straight or a sinuous channel (e.g., Pasquon et al., 2016). New linear dune gullies have been observed to form as well as the lengthening of existing gullies, yet no sinuosity initiation, or sinuosity migration, has yet been reported in linear dune gullies.

1.4 Gully on Matara Crater dunefield

The gully investigated in our study is located on the low albedo intra-crater dunefield of Matara Crater (49.5°S; 34.9°E). These dunes are mainly composed of volcanic sands with basaltic (Paige and Keegan, 1994; Herkenhoff and Vasavada, 1999), or andesitic (Bandfield, 2002) origin. They are likely constituted of sand with a proximal source (Thomas, 1982; Ward and Doyle, 1983). On Mars, dunefields are most common at latitudes above 40°S and around the north polar cap (>75°N) (Hayward et al., 2014). The present-day activity of this gully has been related to the seasonal defrosting of CO_2 (Diniega et al., 2010; Dundas et al., 2012; 2017), but the associated mechanism, the physical state of the CO_2, and the nature and amount of the solid material involved have not been studied in detail.

2 Methods

2.1 Morphology

We performed a detailed survey of one gully using all available HiRISE images of that location. The HiRISE camera, onboard the MRO (Mars Reconnaissance Orbiter) spacecraft, possesses 14 CCD (Charge-Coupled Device) detectors, which operate in the visible (from 536 to 692 nm) and in the infrared (approximately 874 nm) (McEwen et al., 2010). We separated the gully into two areas: 1) the alcove and the beginning of the channel and 2) the channel and the debris apron (Fig. 2D). Changes between images were identified on the RDR (Reduced Data Record) geo-referenced images. The RDR data are calibrated, geo-referenced with change in scale, rotation and translation, and map projected to highlight morphological differences between images. Length, width and area were directly measured on the RDR HiRISE images. Uncertainty on measurements is estimated by determining the reproducibility and the variability of the measurement. Variations in emission angle, roll direction and lighting conditions exist between images and can lead to error in plan-view measurements.

The estimation of the timing of any observed activity is limited by the time sampling of the available observations. Here, we will provide the solar longitude (L_S) of the first image showing a morphological change and the L_S of the preceding image without the change. The duration of surface frost was determined by visual inspection of the HiRISE images. 44 HiRISE images cover the gully studied over 5 Martian Years (MY29-33) with a better temporal coverage in MY30-32.

One HiRISE Digital Terrain Model (DTM) is available for the studied sinuous gully. This DTM was produced from images ESP_022115_1300 and ESP_022392_1300 by the HiRISE team and enable topographic measurements better than 25 cm of relative vertical precision (McEwen et al., 2007). Slope angles were estimated by taking a topographic profile along the line of steepest decent and making a linear fit over the area of interest.

To estimate the erosion and the deposition volume of the Matara dune-gully we used the topographic reconstruction method of Conway and Balme (2014) which consists of estimating the initial topography prior to the gully formation. In brief, we used the topographic contours either side of the gully to estimate the position of the contours across the dune before the gully formed. These contours are then used as

the input to a Natural Neighbor interpolation to produce a gridded elevation dataset. This estimated topography is then subtracted from the real topography to estimate the overall volumes of deposition and erosion. Given the irregular topography of the dune, the errors are likely larger than in Conway and Balme (2014). Therefore in order to estimate the potential errors on this calculation, we linearly connected the contours either side of the gully and re-performed our analysis – we used the difference between these two volumes as an estimate of the magnitude of error.

2.2 Simulation of surface temperature and frost occurrence

We used the one-dimensional energy balance code developed at the Laboratoire de Météorologie Dynamique in Paris (Forget et al., 1999) and modified to simulate ice condensation on sloping terrain with inputs from a general circulation model (Spiga and Forget, 2008; Forget et al., 2008; Vincendon et al., 2010a, 2010b) to assess the climatic conditions on the Matara Crater dunefields.

CRISM (Compact Reconnaissance Imaging Spectrometer for Mars) images were used to inform these simulations. CRISM is an imaging spectrometer with a spatial resolution of 18 m/pixel that covers the visible to infrared wavelengths from 383 to 3960 nm (Murchie et al., 2004). The CRISM images were used to estimate the timing of formation and disappearance of ices using a similar approach to that presented in Vincendon (2015). These timings were refined using small-scale bright frost detections in HiRISE images (Table 1). We then compare these observational constraints to the outputs of a climate model.

Simulations were performed for the pole-facing slope (azimuth = 180°) of an alcove with a slope angle of 24° (cf. active alcove of the sinuous gully, Fig. Suppl. Material 1).

The model outputs are:

- The masses of CO_2 and H_2O ice accumulated on the ground as a function of L_S: these masses are converted to thicknesses using densities of 1.62. 10^3 and 0.92.10^3 kg.m^{-3} respectively.
- The temperature of the surface every half an hour.

Model parameters used for the numerical simulation are given in Table1. Model parameters such as CO_2 ice albedo and ground ice depth are tuned, similarly to Vincendon et al. (2010), to fit the model to the observations of ice previously reported

from near-IR spectroscopy (Vincendon 2015) as well as to the frost occurrence as observed in our study.

Surface albedo			Emissivity		Wind	Thermal Inertia ($J.m^{-2}.s^{-1/2}.K^{-1}$)		Optical depth	Ground ice depth	Frost on HiRISE images	Alcove
sand	*CO_2 ice*	*H_2O ice*	*ground*	*ice*	*($m.s^{-1}$)*	*ground*	*ground ice*	*(change with L_s)*	cm	L_s (°) beginning/end	Θ (°)
0.10	0.4 – 0.65	0.3	0.95	1	10	300	2120	0.46 – 1.17	19	[41.9-56.5 / 183.7-192.3]	24

Table.1. Model parameters used in this study for the numerical simulation of surface temperature and ice occurrence. Dust aerosol optical depth is given at a pressure of 700 Pa and for visible optical depths; it varies as a function of L_s according to an averaged, smoothed scenario derived from Spirit and Opportunity PanCam measurements (Lemmon et al., 2015; Vincendon et al., 2015). Θ is the slope angle and Φ is the azimuth angle.

3 Results

3.1 Overall morphology of the gully with channel sinuosity

The gully studied is located on the eastern part of the Matara Crater dunefield (49.5°S; 34.9°E) (Fig. 2). The dunefield is comprised of transverse dunes and is 16 km across with a low albedo typical of dunes of Mars (Thomas, 1982). The investigated gully is composed of an alcove, a channel, and an apron (Fig. 2D) and measures almost 2700 meters in length (Fig. 2D). The alcove covers a surface area of 3.7 x 10^5 m² and is constituted by 6 sub-alcoves that converge toward the channel. These different sub-alcoves are numbered A_1, A_2, A_3, A_{4a}, A_{4b} and A_5 in Fig. 2E. The channel covers a surface area of 3 x 10^4 m², is ~1000 meters long with a maximum width of 60 m, and has several channel bends. The area of the apron is larger than that of the alcove with a total area of 7.9 x 10^5 m². We estimated a volume of alcove erosion of 6 x 10^6 m³ (+/- 4 x 10^6 m³) and an apron deposit of 8 x 10^6 m³ (+/- 4 x 10^6 m³) (Fig. 3). Within the bounds of the error these two volumes are balanced. In MY29-33 1/5 of the area of the apron experienced changes (Fig. 4D).

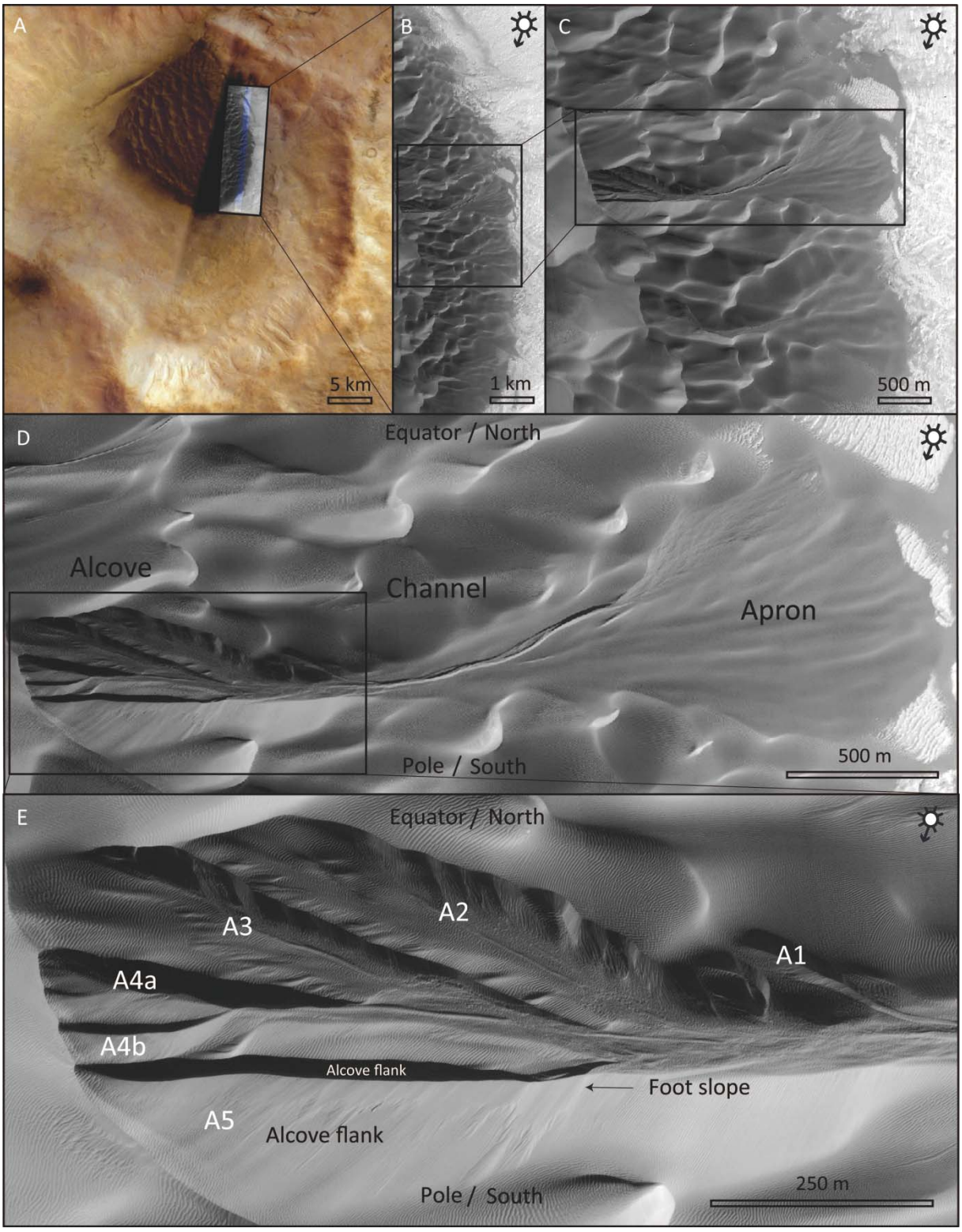

277

278 Fig. 2. A) Matara Crater dunefields (49.5°S; 34.9°E) (Google Mars, HRSC image). B) and C)
279 increasingly detailed view of the eastern part of the dunefield. D) Overview of the sinuous gully on the
280 eastern edge of the Matara Crater dunefield (HiRISE image: PSP_006648_1300 L_s 8.8°). E) Detailed
281 view of the alcove: the different sub-alcove are labelled A_1 to A_5 (B-E: HiRISE image:
282 PSP_006648_1300, L_s 8.8°).

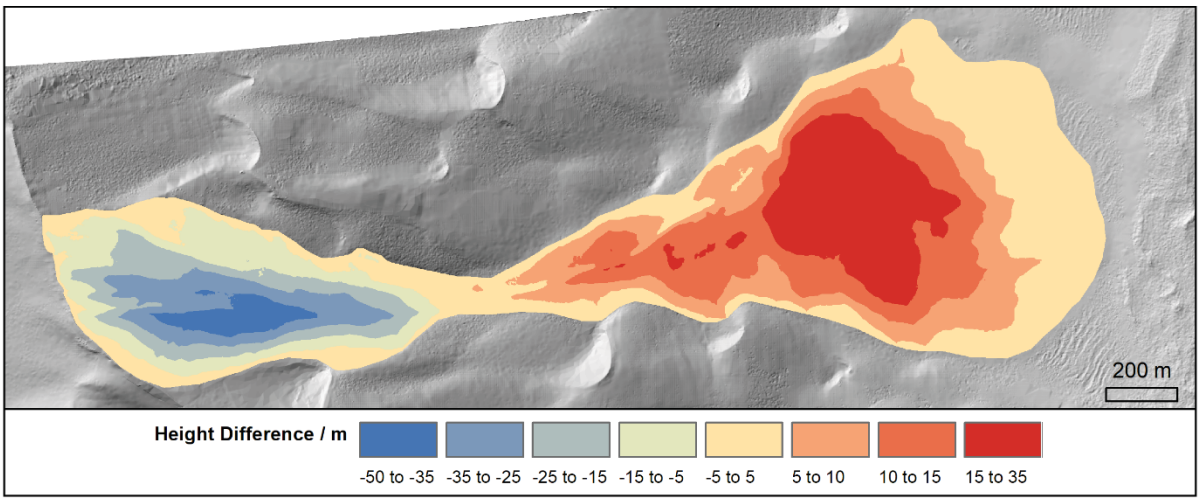

Fig. 3. Estimation of alcove erosion (shades of blue) and apron deposit thickness (shades of red) of the gully on Matara dunefield. The underlying hill shaded relief model is from the publically available HiRISE DTM DTEEC_022115_1300_022392_1300_U01.

3.2 Slopes and cross-sections

Slopes measurements on cross sections and longitudinal profiles were made using the HiRISE DTM. The mean slope of the sinuous gully is ~13°. The alcove has a slope of ~16°, the channel ~13° and the active part of the apron ~10°. The longitudinal cross-section of the gully is slightly concave (Fig. 4A). Two transversal cross-sections are presented: i) at the top of the alcove (Fig. 4B), ii) at the end of the channel (Fig. 4C). The alcove can be separated into different sub-alcoves that we have called: A_1, A_2, A_3, A_{4a}, A_{4b} and A_5 (Fig. 2E) which have different slope angles (Fig. Suppl. Material 1). The morphology of the alcove and its constituent sub-alcoves is asymmetric. For example, in the case of the sub-alcove A_5, the length of the equator-facing flank is greater than that of the pole-facing flank (Fig. 4B). Nevertheless, the average slopes of the opposing sub-alcove flanks are similar: the 6 pole-facing flanks of the sub-alcoves have an average slope angle of 22.8° and the equator-facing flanks have an average slope of 23.2° (Fig. Suppl. Material 1).

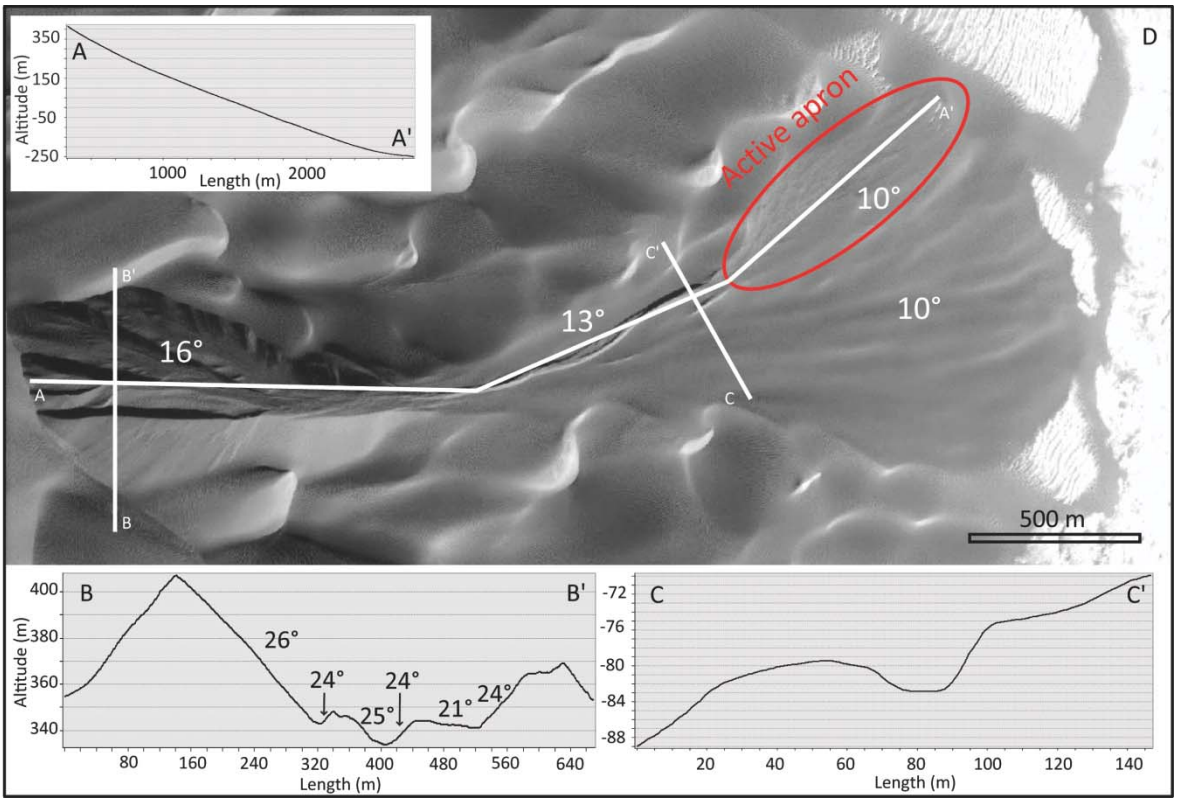

Fig. 4. Topographic profiles of: A-A') along the gully length, B-B') across the upper part of the alcove (the slope along the line of steepest decent of A_5, A_{4a}, A_3 sub-alcoves are marked), C-C') across the lower end of the channel. D) Location of the topographic profiles on the image of the gully (HiRISE image: PSP_006648_1300, L_s 8.8°). Note that vertical exaggeration accentuates some of the slope differences and the slope angles quoted on the cross-profiles are not necessarily measured in the same plane as the displayed profile.

3.3 Evolution in the gully morphology

The studied gully was extremely active during MY29-33. Each year, we observed material transport: inside the alcove, and from the alcove on to the debris apron accompanied by development of sinuosity of the channel. These changes will be summarized in the following sections.

3.3.1 Alcove changes

The alcove of this gully is composed of 6 different sub-alcoves that converge towards the channel: A_1, A_2, A_3, A_{4a}, A_{4b} and A_5 (Fig. 2E). The cross-section in Fig. 4B illustrates the typical topographic configuration of these sub-alcoves. During MY29-33, we observed activity in different sectors of the alcove (Figs. 5ABC; Suppl. Material 2AB). Part of the alcove is considered "active" when a change in the morphology is observed. These changes due to erosion or deposition are easily

observable at the transition between the alcove and the channel of the gully (Figs. Suppl. Material 3; 5ABC; 6AB).

We find that only the activity in the sub-alcoves A_{4a}, A_{4b} and A_5 is temporally correlated with the changes in the sinuosity of the main channel during MY29-33 (Fig. 5). In the next parts, we describe changes in the equator-facing and pole-facing flanks separately, as they have distinctive types of activity.

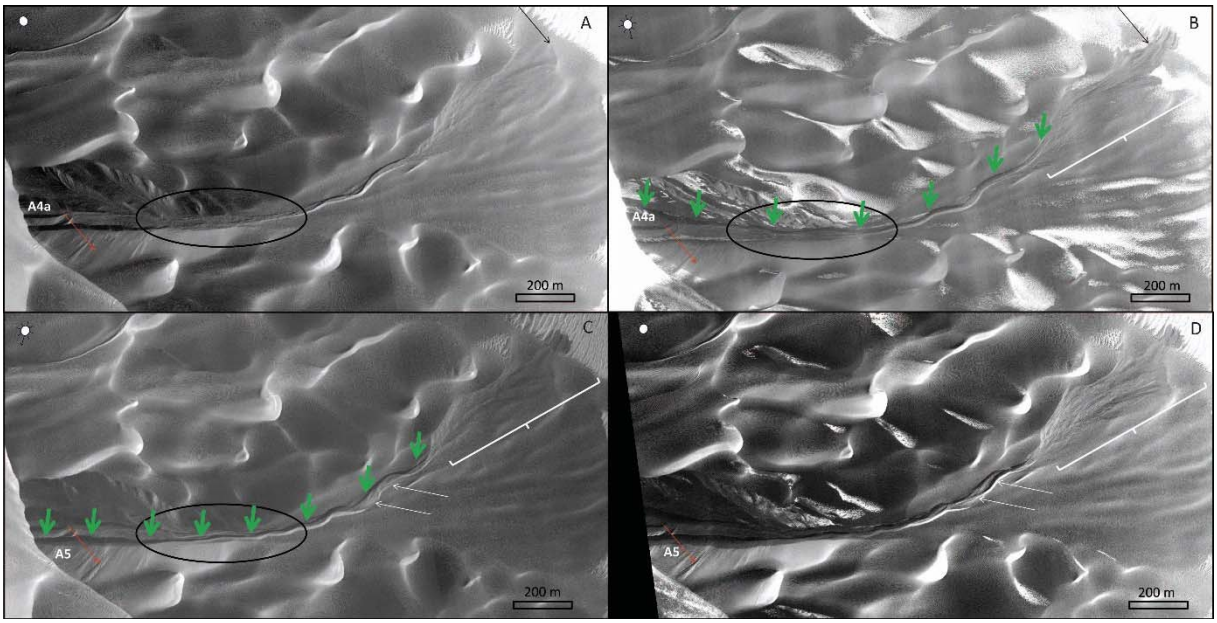

Fig.5. Gully activity over 3 martian years (MY31-33). A) HiRISE image: ESP_046286_1300, L_s 199.8°, MY31: in this reference image the channel is partly filled by sand (black circle). B) HiRISE image: ESP_036910_1300, L_s 144.3°, MY32: the sub-alcove A_{4a} is active (green arrows), a channel is formed (black oval) and material transported onto the debris apron. Subsequent events propagate the channel on the debris apron. C) HiRISE image: ESP_037965_1300, L_s 188.6°, MY32: the sub-alcove A_5 is active (green arrows), a channel is carved (black oval) and modifications occur at the end of the channel and on the debris apron. The red arrows in sub-alcove A_5 indicate a failure scar, under which there is material accumulation. Material has accumulated within the lower part of the channel, which can be explained by the obstruction provided by the previous set of deposits, propagating channel fill upstream. D) HiRISE image: ESP_046238_1300, L_s 167.0°, MY33: the material accumulated in the sub-alcove A_5 is transported onto the channel and the debris apron. Material continues to accumulate within the lower part of the channel, blocked by the previous deposits, propagating channel fill upstream. White arrows show where modification of the channel morphology has occurred. Thin arrows are reference points: red arrows for material accumulation, black arrows for material transport onto the debris apron, and white arrows for changes in the channel morphology. Thick green arrows indicate where there is activity in the alcove and channel of the gully. Black ovals highlight changes in

morphology in the area between the alcove and the beginning of the channel. White brackets show multiple overlapping deposits.

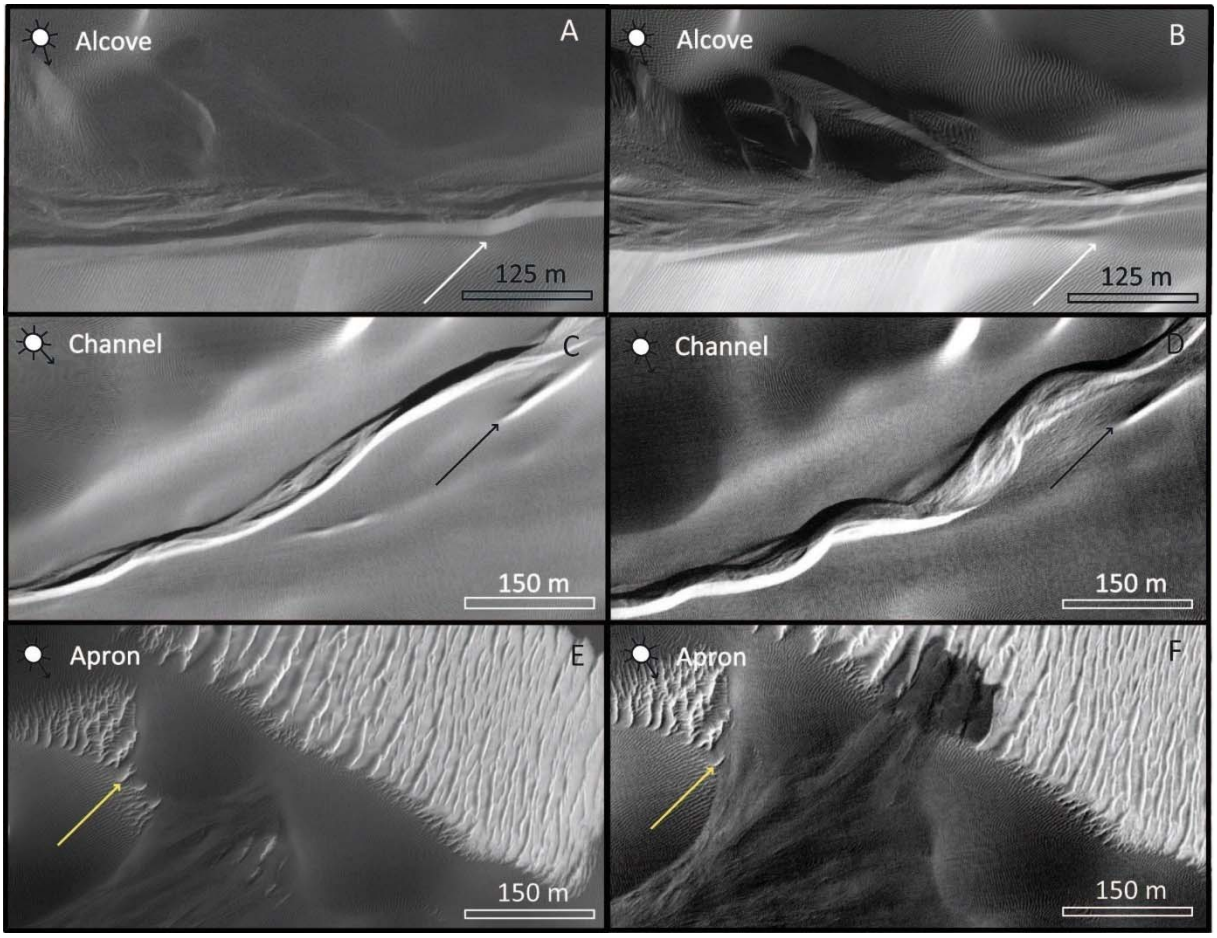

Fig. 6. Summary of main gully activity types represented by before-after pairs of images. (A-B) At the transition between the alcove and the channel, sediment erosion and accumulation alternates, causing channel formation, partial channel infilling or complete channel erasure. A) HiRISE image: ESP_028972_1300, L_s 180.8° (MY32). B) HiRISE image: ESP_037965_1300, L_s 188.6° (MY32). (C-D) Development of a more sinuous channel. C) HiRISE image: ESP_006648_1300 L_s 8.8° (MY29). D) HiRISE image: ESP_037965_1300, L_s 188.6° (MY32). (E-F) Elongation of the debris apron deposits. E) HiRISE image: ESP_034009_1300, L_s 41.8° (MY32). F) HiRISE image: ESP_037411_1300, L_s 164.5° (MY32). The white arrow shows a reference point between images A and B, the black arrow between images C and D and the yellow arrow between images E and F.

3.3.1.1 Equator-facing flanks: material accumulation in the alcove

Sand material transport and accumulation was observed in sub-alcoves A_{4a} to A_5 (Figs. 7; 5). Material transport is only observed on the equator-facing flanks (Figs. 7; 5C; Suppl. Material 3). On the equator-facing flanks of sub-alcoves A_{4b} to A_5, small discrete slope failures oriented toward NNE result in the transport of sand material that is identifiable as accumulations on the alcove floors (Figs. 7ABC; 5C; Suppl.

361 Material 3). These failures comprise an alcove or scar and an apron, sometimes
362 connected by a depression, or channel (Figs. 7C; 5C; Suppl. Material 3). The total
363 area affected by these failures ranges between 2000 and 8000 m^2 and is highly
364 variable from one year to the next (Fig. 7D). During MY29-33, the cumulative area
365 affected by material transport and accumulation in the alcove attains 31 800 m^2 (Fig.
366 7D). An area of 14 800 m^2 is affected by material accumulation on the floor of the
367 sub-alcove A_5. The material initially accumulated in sub-alcoves A_{4b} to A_5 was
368 transported onto the debris apron of the gully (Fig. 5). This transport causes erosion
369 and deposition of sediment and the creation of a channel in the terminal part of the
370 alcove (Figs. Suppl. Material 3; 5ABC; 6AB).There was no observed accumulation of
371 material for MY29-33 in sub-alcoves A_1 to A_3 (Figs. 2E; 5), and no channel changes
372 were observed during their defrosting.
373

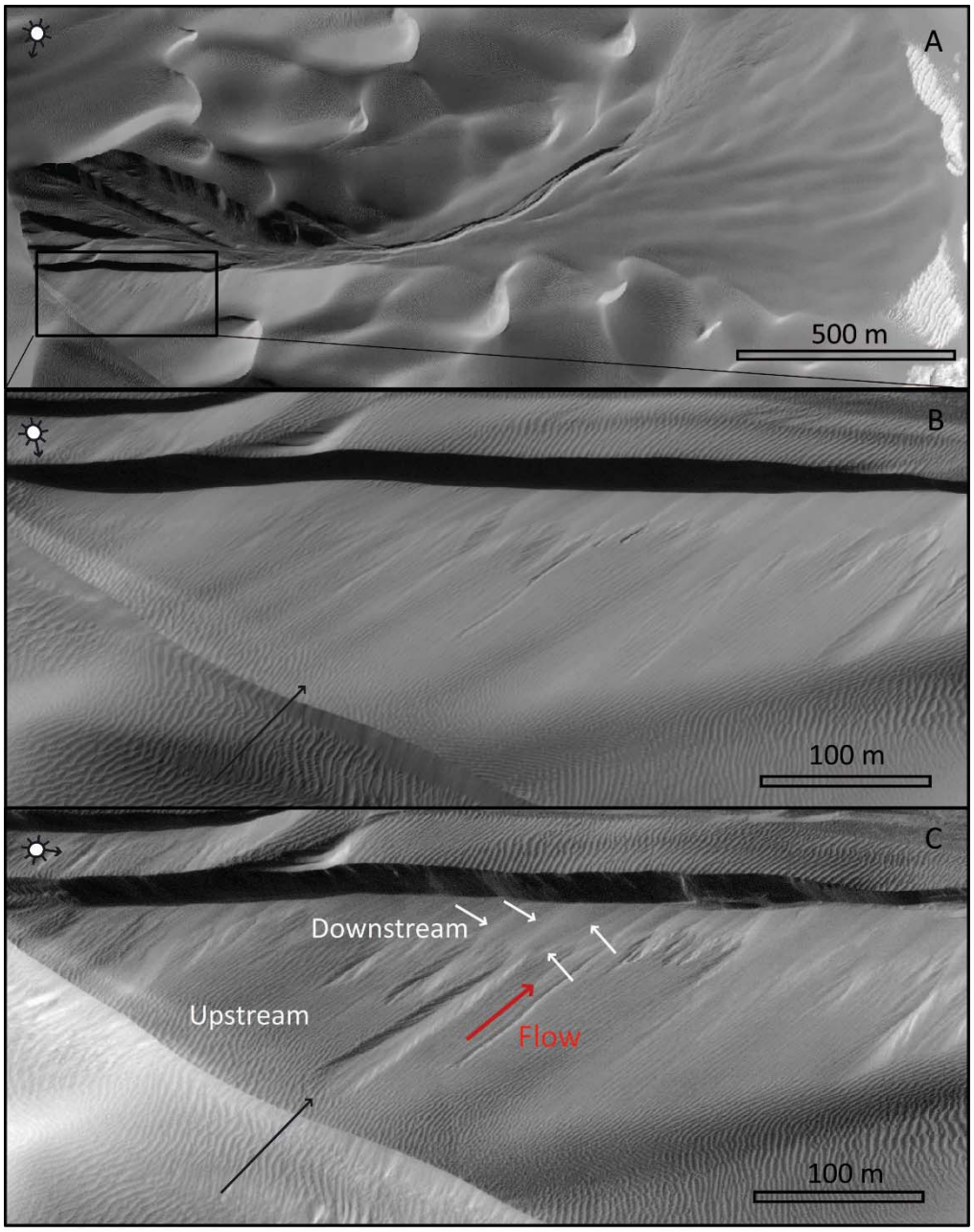
A
500 m
B
100 m
C
Downstream
Upstream
Flow
100 m

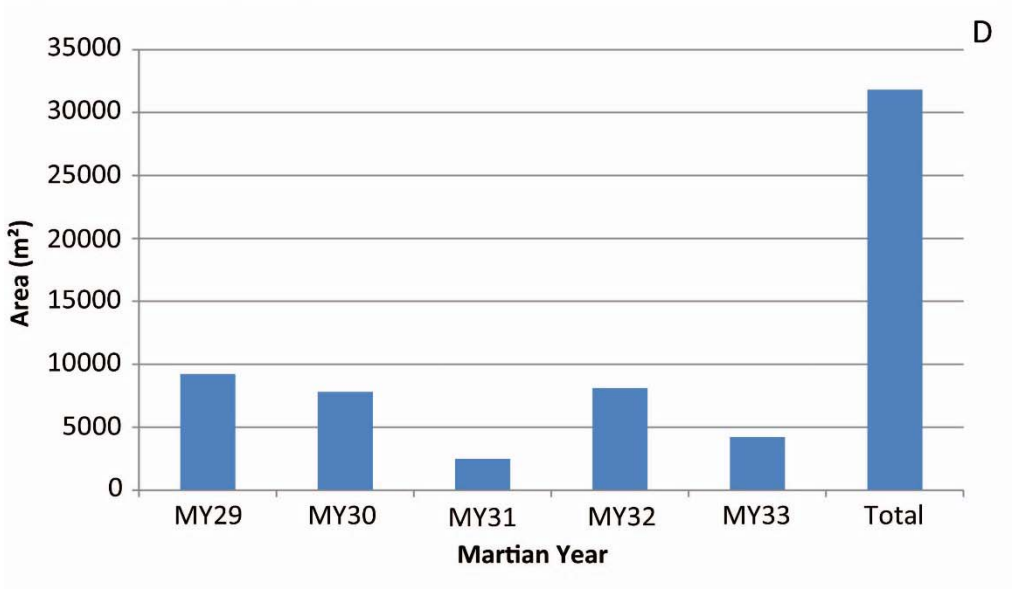
D
35000
30000
25000
20000
15000
10000
5000
0
Area (m²)
MY29
MY30
MY31
MY32
MY33
Total
Martian Year

374

Fig. 7. A) Context view of the gully on the Matara Crater dunefield (HiRISE image: PSP_006648_1300 L_s 8.8°). B) and C) Detailed view of sub-alcoves A_{4b} and A_5, showing before and after examples of the failures resulting in erosion of the flanks and accumulation on the alcove floor (HiRISE image: PSP_006648_1300, L_s 8.8° MY29 and ESP_029394_1300, L_s 199.8° MY31). The black arrow indicates a reference point and the white arrows the location of accumulated material. D) The total area affected by the failures in the sub-alcoves A_{4a} and A_5 for MY29 to 33, including the erosional scar, the transport zone and the deposited material.

3.3.1.2 Pole-facing flanks: frost and collapse of material

Seasonal frost deposits appear each year during the winter season on some parts of the sinuous gully studied, but not everywhere. These deposits are visible on HiRISE images. This ice can be observed on the alcove, specifically on the pole-facing flanks of each sub-alcove (A_1 to A_5) (Figs. 8AC; 5B). For sub-alcoves A_{4a}, A_{4b} and A_5, seasonal frost is only present on the pole-facing flank (Suppl. Material 2CD), for the other sub-alcoves frost is also visible on the equator-facing flanks (Figs. 8AC; 5B). The appearance and disappearance of frost is generally gradual for the sub-alcoves of this gully (Fig. 8), except for some events in sub-alcoves A_{4a}, A_{4b} and A_5 where the defrosting is sudden and contemporaneous with channel and apron activity, described in Section 3.3.2. (Fig. 8). This sudden defrost coincides with the collapse of part of the alcove flank (Fig. 8).

We observe alternation in the activity of the sub-alcoves A_4 and A_5 (Fig. 5), so the source of the material driving changes downstream in the gully differs over time.

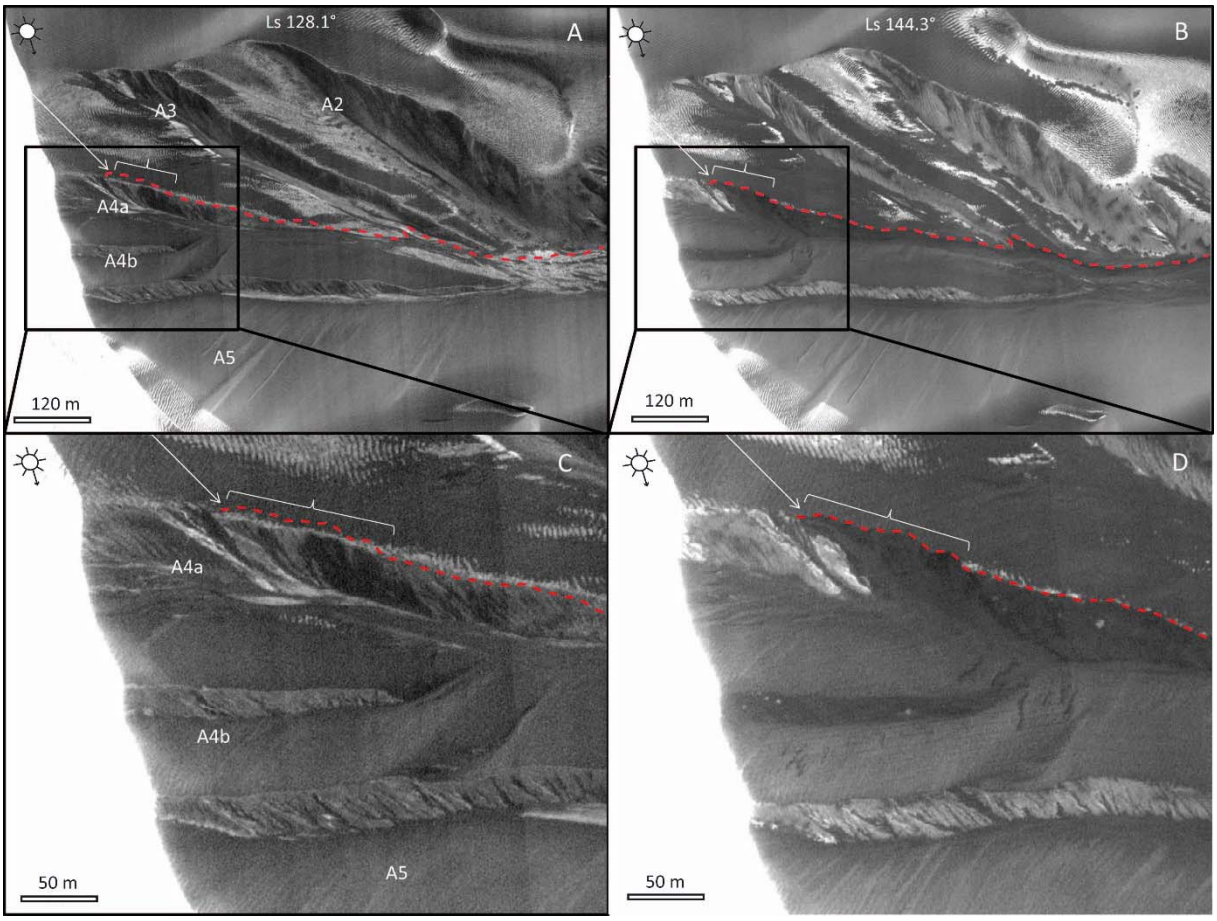

Fig. 8. Alcove activity. A) The gully alcove in the middle of winter; seasonal frost is observed mostly on the south-facing flanks of the alcoves, HiRISE image: ESP_036488_1300, L_s 128.1°. B) Collapse of one part of the sub-alcove A_{4a}. The seasonal frost disappears from pole-facing flank of the sub-alcove A_{4a} and material is transported toward the debris apron, HiRISE image: ESP_036910_1300, L_s 144.3°. C) Detailed view of sub-alcoves A_{4a} and A_{4b} from panel A. D) Detailed view of sub-alcoves A_{4a} and A_{4b} from panel B. The white arrow indicates a reference point, the white bracket shows the area of collapse visible in panels B and D, and the red dotted line shows the extent of the activity in sub-alcove A_{4a}: all parts of the slope below the line are affected by material collapse (changes are visible in panels B and D).

3.3.2 Channel and apron changes

3.3.2.1 Channel changes

We observed that channel sinuosity initiated and increased during MY29-33 in this gully system. The sinuosity of the channel is quantified using the sinuosity index "S" (Fig. 9). In our first observations during MY29 the channel was sub-linear with a sinuosity index of 1.0098 (Figs. 10A; 9). During MY30, one part of the channel was abandoned and the channel developed some curvature as indicated by an increase in the sinuosity index to 1.018 (Figs. 10B; 9). In MY31, the sinuous section developed

greater curvature and two terraces appeared on the inside of the bend. The sinuosity index reduced to 1.006 (Figs. 10C; 9). In MY32 four bends are visible and sinuosity increased reaching the maximum value of 1.05; (Figs. 10D; 9). Finally during MY33 these bends migrate and part of the channel was abandoned. The sinuosity index remained stable at 1.05 (Figs. 10E; 9). The lateral bend migration rate is ~ 23 m/yr calculated on a baseline between L_s 8.8° in MY29 and L_s 188.6° in MY32. The width of the channel grew from 30 m in MY29 to more than 60 m in MY33.

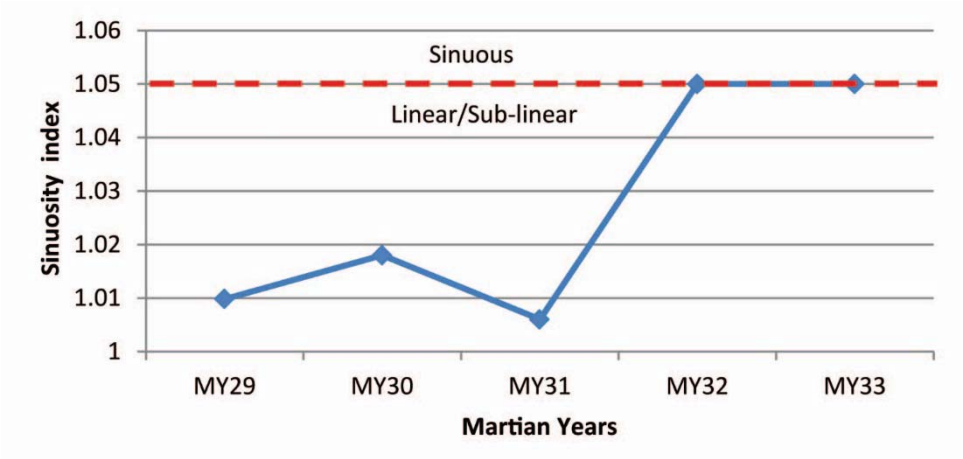

Fig. 9. Change in the sinuosity index of the channel over 5 martian years (MY29-33).

We observed an upstream propagation of the channel bends. We observed the formation of terraces with point bar deposits (Fig. 10BC) and their disappearance (Fig. 10DE), which demonstrates active erosion and deposition in the channel. We observed a cycle of transport and backfill. Each pulse of activity transports material downstream, resulting in the infill of the channel near the apron. As a consequence, the next pulse can be blocked by this obstacle and the channel infill propagates upstream (Fig. 5CD). Subsequent events can break through this infill and the cycle repeats (Fig. 5B). The channel extended more than 140 m in one single year (MY32) for a total length of 800 m (Figs.11A; 6F; 5B).

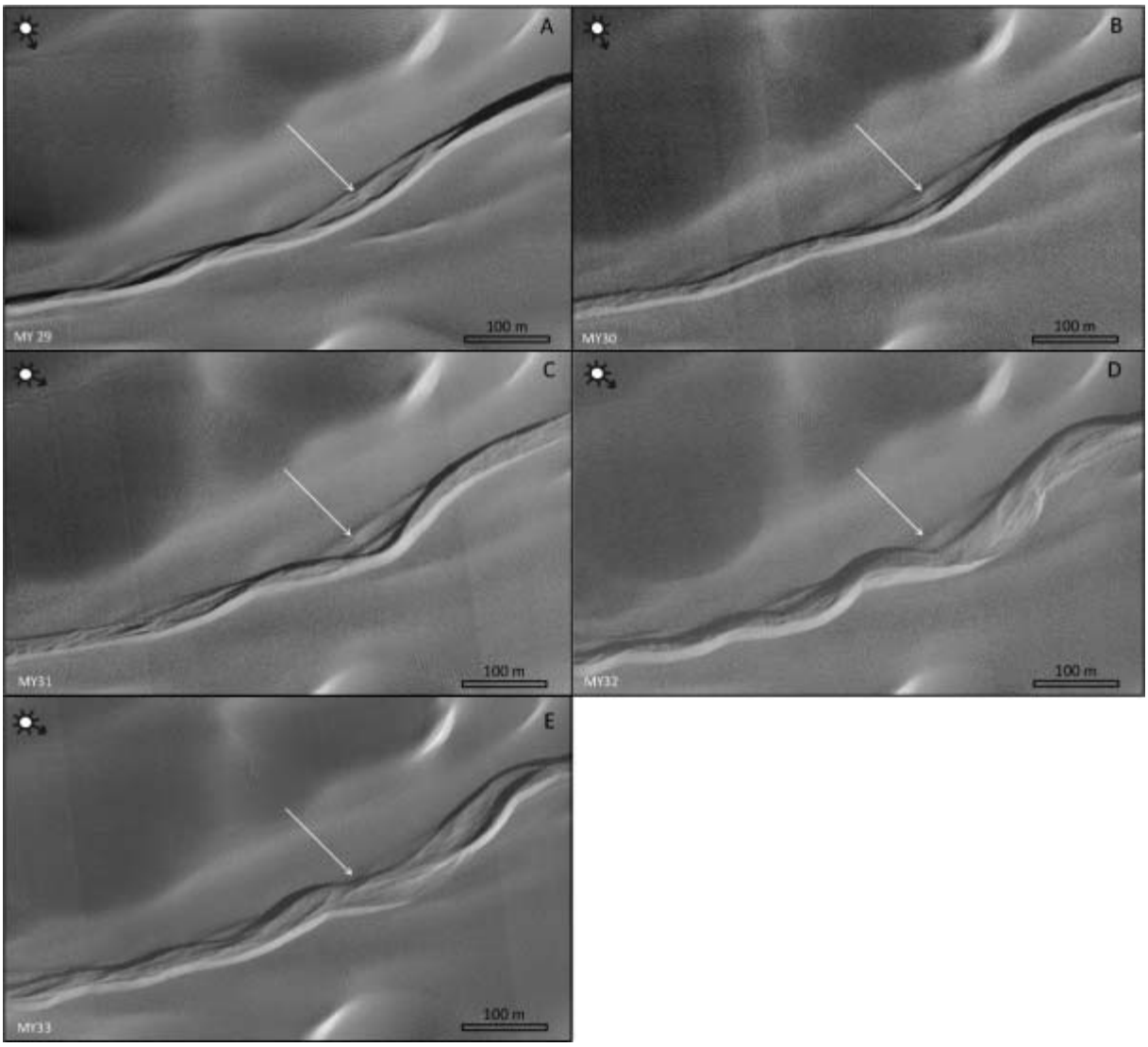

Fig. 10. Changes in the gully channel over 5 martian years (MY29-33). A) HiRISE image: PSP_006648_1300, L_s 8.8° (MY29), B) HiRISE image: ESP_020559_1300, L_s 198.9° (MY30), terrace formation with point bar deposits, C) HiRISE image: ESP_029394_1300, L_s 199.8° (MY31), terrace formation with point bar deposits, D) HiRISE image: ESP_037965_1300, L_s 188.6° (MY32), terrace erasure, sinuosity index of the channel reaches 1.05, E) HiRISE image: ESP_046853_1300, L_s 191.8° (MY33), terrace erasure, sinuosity index of the channel stable at 1.05. The white arrow shows a reference point and situates the point bar deposits.

3.3.2.2 Debris apron changes

The modification of the debris apron was characterized by measuring the length (Fig. 11A) and the area changes (Fig. 11B) of the new deposits. These changes happened at the same time as the channel changes documented above (Figs. 5AB; Suppl. Material 2AB). The apron deposits can extend by up to ~140 meters over their previous extent in one martian year (Figs. 11A; 6EF; 5AB). MY32 shows the most extensive activity on the gully apron in terms of length propagation

(Fig. 11A). Only the northern part of the apron was active over MY29-33 (Figs. 4D; 5). We observed the development of multiple overlapping deposits (Fig. 5BCD). Between L_s 283.3° MY29 and L_s 144.3° MY32 the activity of the apron was characterized by the appearance of new deposits without any lengthening (Figs. 11A; 5CD). An average 1.7 x 10^5 m² of the apron surface is affected by the gully activity during MY29-33 (Fig. 11B). This area represents around 20% of the total apron area (7.9 x 10^5 m²), suggesting such activity has been ongoing, perhaps on the order of decades.

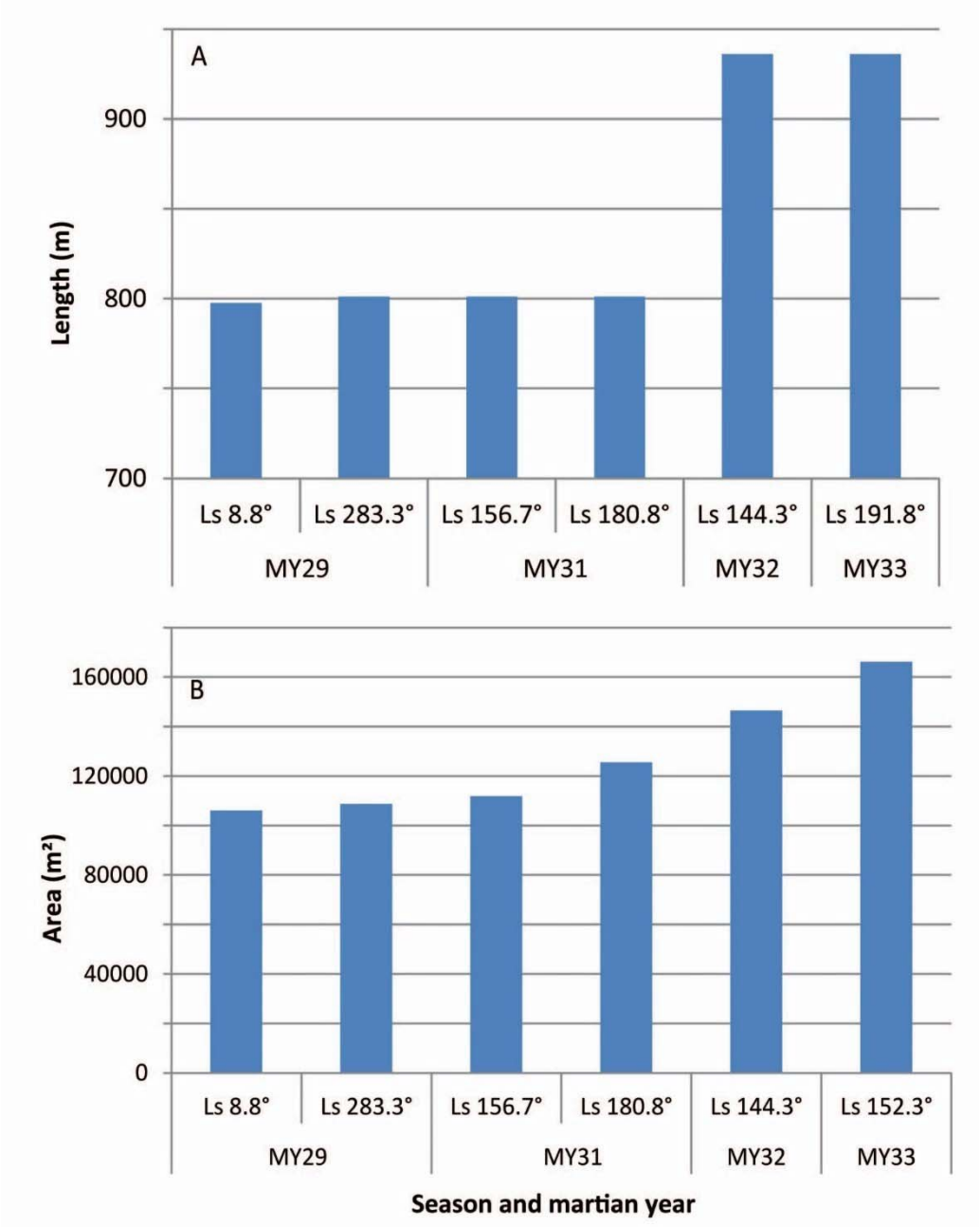

Fig. 11. A) Changes in the active apron length (+/-10m). B) Changes in the active apron area (+/-100 m²) over 4 martian years. Image quality in MY30 did not allow us to make measurements on the debris apron.

3.4 Timing of activity

3.4.1 Timing of alcove activity (A_{4a}, A_{4b} and A_5)

3.4.1.1 Material accumulation (Equator-facing flanks)

On the equator-facing flanks of the sub-alcoves A_{4a}, A_{4b} and A_5, we observed material transport and accumulation on the alcove floors (Figs. 7; 5C; Suppl. Material 3). During MY30, this activity occurred throughout the period spanning the beginning of winter until the middle of spring (i.e., between L_s 56.5° and 249.9°) (Fig. 12A). For MY31, the activity was observed between L_s168.8° at the end of winter and L_s199.8° at the beginning of spring (Fig. 12A). In MY32, it occurred at the end of winter between L_s 164.5° and L_s 176.4° (Fig. 12A). For MY33, it started during the middle of winter at L_s 152.3° and was still ongoing at the beginning of spring at L_s 191.8° (Fig. 12AE).

In general, material accumulation in the alcoves occurs between the beginning of winter and the middle of spring (Fig. 12E). We did not observe seasonal frost on HiRISE images at the location where the material transport occurs (Figs. 8AC; 5B; Suppl. Material 3). This type of activity in the alcove is never observed during summer and autumn in the time period studied, MY29-33 (Fig. 12AE). However, only a few images are available between mid-spring and mid-autumn, which may bias our observations. Moreover, we observe that this activity has a highly variable timing from one martian year to the next (Fig. 12AE).

3.4.1.2 Seasonal frost (Pole-facing flanks)

Seasonal frost is only observed on the pole-facing flanks for sub-alcoves A_{4a}, A_{4b} and A_5. This frost is visible from L_s 95.2° to L_s 141.8° during MY30, between L_s 67.5° and L_s 156.7° during MY31, between L_s 56.4° and L_s 144.3° during MY32 and finally, from L_s 149.7° to L_s 167.0°, during MY33 (Fig. 12D). So, for MY29-33 seasonal frost is temporally well constrained and observed between the middle of autumn and the middle of winter, between L_s 67.5° and L_s 167.0° (Fig. 12DE). The detailed presence of frost on sub-alcoves A_{4a}, A_{4b} and A_5 is presented in Supplementary Material Fig. 2CD. No seasonal frost is observed on the equator-facing flank of sub-alcove A_5 for MY29-33, where material transport and accumulation is usually observed (Fig. 12B).

3.4.2 Timing of the channel and the apron activity

Changes in the channel and the apron are originate from sub-alcoves A_{4a}, A_{4b} and A_5.These changes occur contemporaneously at the beginning of winter, at L_s 117.6° in MY30. During MY31, the changes occur between the middle of winter and the beginning of spring, i.e. between L_s 156.7° and L_s 180.8°. During MY31, the changes are observed in the middle of winter between L_s 144.3° and L_s 158.5°. Changes occur between L_s 149.7° and L_s 152.3° for MY33 (Fig. 12CE). When there is more than one pulse of activity per year, these pulses originate from different sub-alcoves (Figs. 5BC; Suppl. Material 2AB). We conclude that the activity of the channel and of the apron is well constrained and occurs each year from winter to the beginning of spring between L_s 117.6° and L_s 180.8° during MY29-33 (Figs. 12CE; Suppl. Material 2AB).

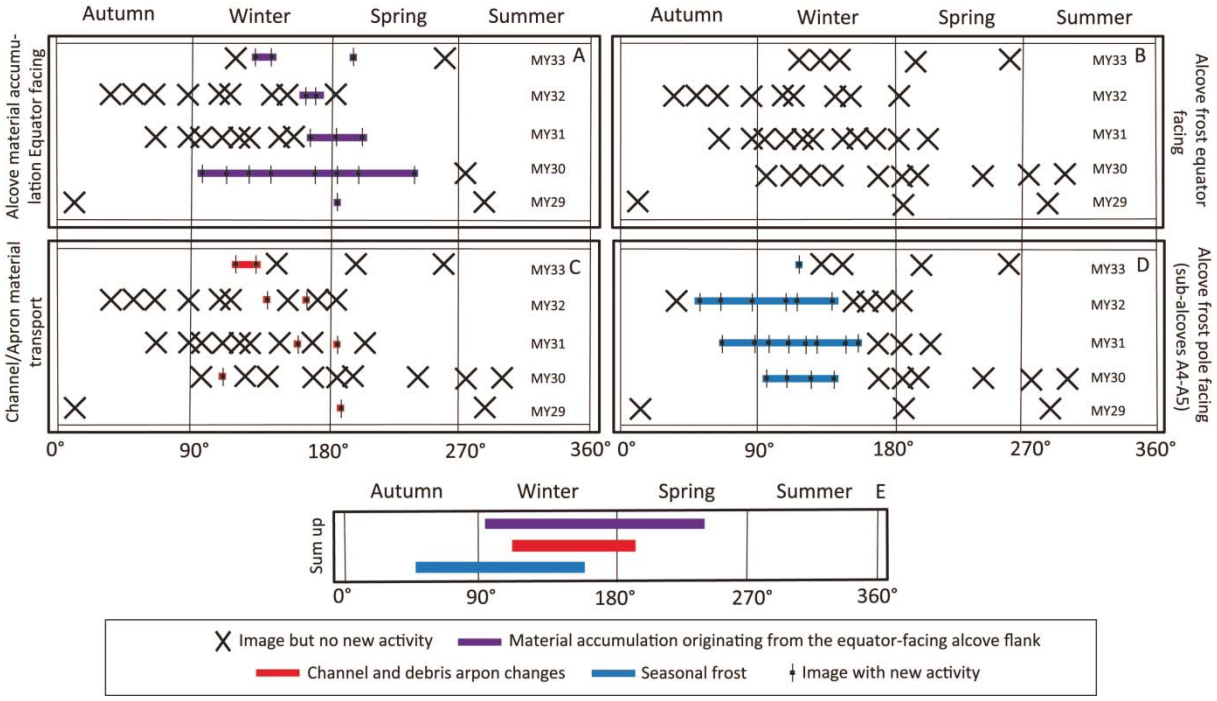

Fig. 12. A) Timing of material transport inside the alcove, including only sub-alcoves A_{4a}, A_{4b} and A_5 where material accumulation on the floor of the alcoves can be identified, sourced from failures on the equator-facing flanks. B) Timing of presence of seasonal frost for sub-alcoves A_{4a}, A_{4b}, A_5 on their equator-facing flanks. C) Timing of activity for material transport from the alcove to the apron accompanied by changes in channel sinuosity. D) Timing of the presence of seasonal frost for sub-alcoves A_{4a}, A_{4b}, A_5 on their pole-facing flanks. Each line represents one martian year and each cross is a HiRISE image. E) Summary of the information presented in panels A-D.

3.4.3 Timing synthesis

Each year we observed: i) material transport from the equator-facing flanks of the sub-alcoves A_{4a}, A_{4b} andA_5 to their floors, between the beginning of winter and the middle of spring (Fig. 12AE), ii) seasonal frost on the pole-facing flanks of the alcove between the middle of autumn and the end of winter (Figs. 12DE; Suppl. Material 2CD), iii) sudden disappearance indicating collapse of the frost on pole-facing alcove flanks contemporaneous with changes in the channel and debris apron (Figs. 12; Suppl. Material 2). The activity observed in the channel and on the debris apron can occur during winter up until the beginning of spring (Figs. 12CE; Suppl. Material 2AB).

3.5 Modeled temporal evolution in surface temperature and seasonal frost composition and thickness

3.5.1 Seasonal frost deposits

Seasonal frosts occur each year on the Matara Crater dune-gully, particularly in the alcove and on the pole-facing flanks of the sub-alcoves A_{4a} to A_5 (Figs. 8AC; 5B). These sub-alcoves are the source of the material that then cause changes in the channel sinuosity and changes on the debris apron. Defrosting of the seasonal ice deposits is thought to play a role in present-day gully activity (e.g., Dundas et al., 2012; 2015; 2017; Diniega et al., 2013) so, we studied frost composition and thickness using a modelling approach calibrated with HiRISE and CRISM data (see section 2.2). The results of the simulations for the pole-facing flank of the sub-alcove A_5 are shown in Fig. 13. The simulations predict that CO_2 frost begins to deposit in the middle of autumn at L_s ~40-60°. The CO_2 ice thickness increases to a maximum of 85-130 mm near mid-winter (L_s 140°-150°). After ~ L_s 150°, the CO_2 ice thickness decreases and the CO_2 frost totally disappears at L_s ~180-190° (Fig. 13A).

Our simulation suggests that H_2O ice is also present in the seasonal frost, but in smaller quantities (i.e., ~10-11 µm thickness). Such a low thickness of water ice is close to the detection limits of near infrared spectroscopy of ~ 5 µm (Vincendon et al. 2010b). The simulations predict that water ice first appears at L_s ~20° at the beginning of autumn, while evidence for ice in the observations are found at L_s > 80° only, which is consistent with the predicted low thickness of water ice that remains around 5 µm from L_s 30° to L_s 150° in the model (Fig. 13A). At L_s 150°, the model shows an increase in the H_2O ice thickness to 10-12 µm lasting until L_s 195°, which is supported by observations of ice over most of that period. At this point, the H_2O ice

548 thickness decreases reaching 0 μm at L_s ~200°. In summary, H_2O ice is predicted to
549 be present between L_s 20° to L_s 195°- 200°, i.e., from the beginning of autumn to the
550 beginning of spring. Once CO_2 has disappeared, the model predicts that some water
551 ice remains for a few days (Fig. 13A), a phenomenon that is predicted to occur
552 frequently on Mars although it has never been observed, probably due to a lack of
553 appropriate timing of observations (Vincendon 2015).

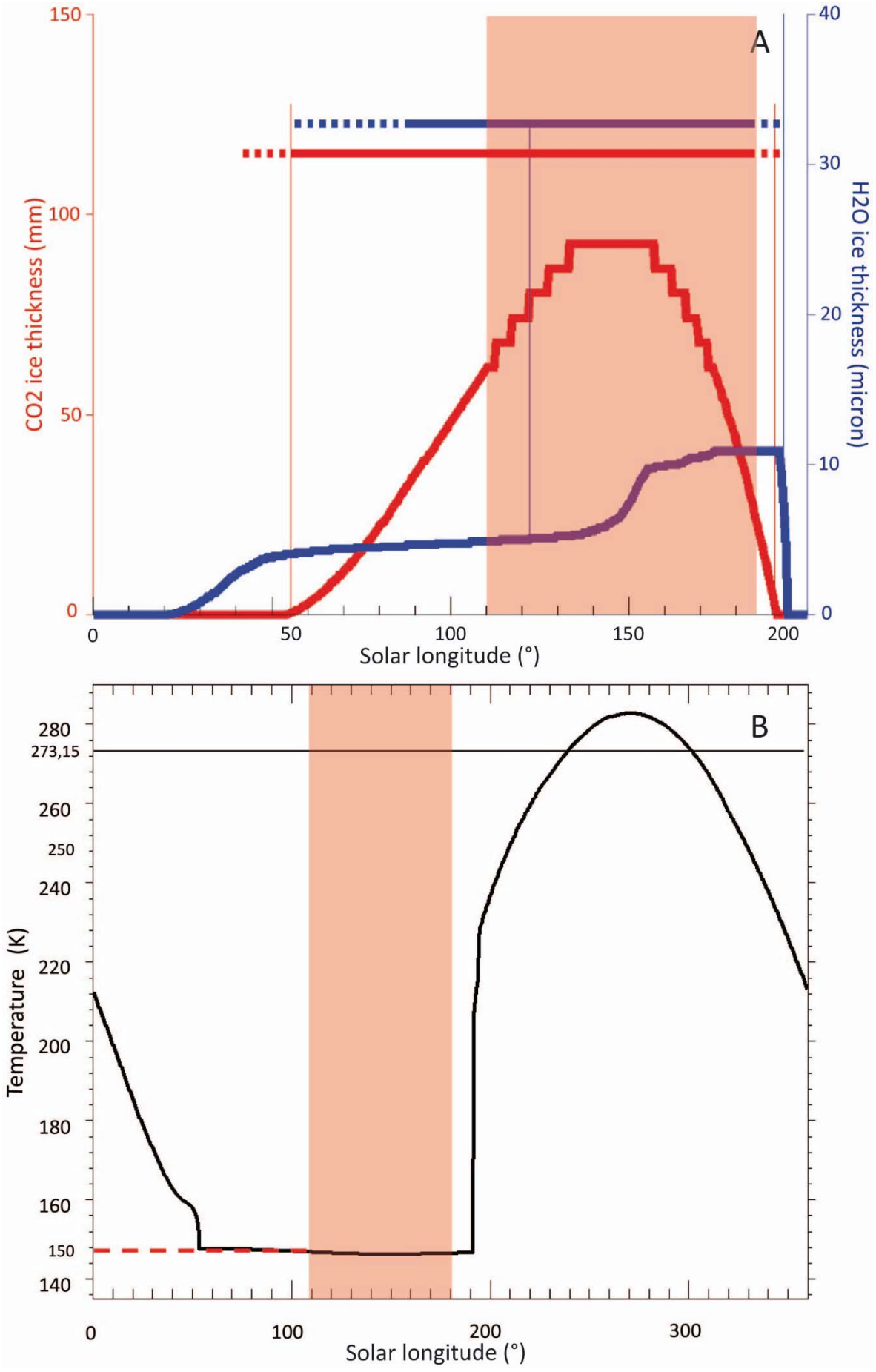
A
CO2 ice thickness (mm)
H2O ice thickness (micron)
Solar longitude (°)
B
Temperature (K)
273,15
Solar longitude (°)

554

Fig. 13. Numerical simulation results for the Matara Crater dunefield (49.5°S; 34.9°E) for pole-facing flanks of the sub-alcove A_5 with 24° slope: A) Composition and thickness of the seasonal frost predicted to be present. The red line shows the CO_2 ice frost thickness (mm) and the blue line shows the H_2O ice thickness (μ). B) Modeled surface temperatures (predicted by the model at 2 pm local time). Temperatures are calculated with a time step of 30 minutes over one martian year. The orange area highlights the period during which channel and apron changes were observed (summarized in Fig. 12).

3.5.2 Surface temperature

Simulations of surface temperature were performed in the same location where frost composition and thickness simulations were performed (Fig. 13B). We observed changes in the channel and apron between L_s 117.6° and L_s 180.8° (Fig. 12CE), a period where the alcove is covered by CO_2 ice and during which the model predicts a temperature of about 145-150 K (Fig. 13B). The model shows that during the few days (sols) following the disappearance of CO_2, and once the water ice has disappeared, the temperature of the pole-facing flank quickly increases to reach 240K at L_s 200°. Note that these changes in frost and temperature do not concern the adjacent, non-pole-facing, and thus warmer, areas of the alcove.

4 Interpretation and discussion

The transport of material from the alcove to the debris apron is contemporaneous with: modifications on the alcove floor, the increase in channel sinuosity, and the modification of the channel and the apron (Figs. 6; 5).

4.1. Material accumulation and alternating source

Two points seem necessary for the development of sinuosity: 1) material accumulation on the floor of the alcoves of the gully and 2) the alternation of the active sub-alcove.

The sub-alcoves A_1 to A_3 do not show any activity that can be linked to the sinuosity development in the gully channel. We do not observe any material accumulation in these sub-alcoves. Sub-alcoves A_4 to A_5 do show material accumulation which is transported in winter through the channel and onto the debris apron of the gully.

We do not think that the properties of the material into which the flow is eroding is directly responsible for the development of sinuosity because there are many non-sinuous gullies observed on other sand dunes (Diniega et al., 2010;

588 Pasquon et al., 2016). However, erosion of material is a necessary to explain terrace
589 formation and suggests that the material must be sufficiently unconsolidated to be
590 incorporated in the flow.

591 We observe alternating activity in sub-alcoves A_4 and A_5 (Fig. 5). The material
592 transported through the channel and onto the debris apron of this gully does not
593 originate from exactly the same area of the alcove from one active period to the next
594 (Fig. 5). This could cause in homogeneities in the spatial distribution of erosion and
595 deposition in the channel initiating the development of channel sinuosity.

596 ### 4.2. Transport process

597 We hypothesize that the increase in channel sinuosity of the Matara Crater
598 dune-gully is due to: 1) an alcove material contribution with alternation/variation of the
599 alcove source location (A_4 to A_5) and 2) a flow process that produces landforms
600 similar to those created via terrestrial hyper-concentrated flows, as outlined below.

601 To try to understand the processes behind the present-day activity in the gully
602 on Matara Crater dunefield, we compare our observations with the properties of three
603 different processes which are known to produce channel bends, or sinuosity on
604 Earth: river meanders, hyper-concentrated flows and debris flow (Table 2).

Morphological observations of the gully on the Matara Crater dunefield	**Terrestrial river meanders**	**Terrestrial hyper-concentrated flows**	**Terrestrial debris flows**
Material accumulation on one side and erosion on the other side of the channel	X	X	-
No levees	X	X	-
Sinuosity migration	X	X	-
Formation mode: instantaneously	-	-	X
Point bar deposits and lateral migration	X	X	-
Evolution from straight to sinuous	X	X	-
Upstream accumulation	X	X	X
Significant amount of solid material	-	X	X

Table 2. Comparison between the sinuous gully studied on Mars and the behavior/morphology of three others processes which can develop channel sinuosity on Earth (Leopold and Wolman, 1960; Hickin, 1974; Pierson, 1981; Allen, 1985; Williams, 1986; Johnson et Rodine, 1984; Coussot et Meunier, 1996; Allen, 1997). Crosses indicate that the terrestrial analogues possess similarities with the stated properties for the gully on the Matara Crater dunefield and "-" indicates dissimilarity.

Debris flow processes have been proposed as a possible formation explanation of gullies on Mars (Costard et al., 2002; Mangold et al., 2003; Jouannic et al., 2012; 2015). Table 2 shows that very few of the morphological attributes and behavior of the gully on the Matara Crater dunefield are consistent with observations of terrestrial debris flows. There are more morphological and behavioral similarities with meandering rivers and hyper-concentrated flows. The formation mode of a terrestrial meander is in a permanent flow of water. However, abundant liquid water cannot exist under present-day martian conditions: the pressure, temperature and humidity conditions are too low (Hecht, 2002), so we discount this formation process.

Hyper-concentrated flows seem to be the best potential analogue for the activity observed in the sinuous gully on Matara Crater dunefield, because they have the most similarities in Table 2. On Earth, hyper-concentrated flow is defined as a two-phase flow of water and sediment, intermediate in concentration between normal streamflow and debris flow or mudflow (Pierson, 2005). The suspended sediment concentration ranges between 20 and 70% (Pierson, 2005; Allen, 1997). However, such a mechanism requires large quantities of liquid water which are inconsistent with present-day martian atmospheric conditions, as described above for meanders. It is possible that the morphologies produced by a hyper-concentrated water flow could also be produced by an alternative fluid, as discussed below.

4.3. Role of CO_2

Our observations of timing and location of the activity producing a sinuous channel suggest that the activity is linked to the seasonal defrosting of CO_2 ice (Figs. 8; 12CDE; 13A; 5; Suppl. Material 2). However, the exact relation between CO_2 ice and the numerous seasonal surface processes temporally linked to its defrosting on Mars is not fully understood (e.g., Dundas et al., 2012; Harrison et al., 2015; Pasquon et al., 2018).

Sublimation of seasonal CO_2 ice on martian dunes is thought to trigger the formation of dark spots and dark flows (Kieffer, 2000; 2007; Piqueux et al., 2003; Kieffer et al.,

638 2006; Piqueux and Christensen, 2008). These morphologies have no measurable
639 topographic effect (Hansen et al., 2011; Raack et al., 2015). Sublimation of CO_2 ice
640 has also been associated with meter-scale topographic changes observed in “classic”
641 mid-latitude gullies (Pilorget and Forget, 2015; Vincendon, 2015; Dundas et al.,
642 2017). The feasibility of this process as an agent of topographic change has been
643 also been suggested by recent laboratory experiments showing that small amounts of
644 CO_2 frost deposited into a granular medium can cause granular flows on slopes >13°
645 under terrestrial gravity (Sylvest et al., 2015; 2018). However, these experiments did
646 not test whether the subsequent flow would have enough energy to move the bed
647 materials over low slopes for tens to hundreds of meters.
648 Our numerical simulations predict that CO_2 should be present on pole-facing alcove
649 flanks between L_s 40-60° and L_s 180-190° (the middle of autumn to the beginning of
650 spring) on the Matara Crater dunefield (Fig. 13A).The remobilization of the material
651 accumulated on the alcove floor is associated with collapse of the pole-facing alcove
652 flanks which happens at a time of year when our modeling predicts that the CO_2 ice
653 should be at its thickest (Figs. 8; 13A). The changes in channel and apron
654 morphology of the gully occur in winter between L_s 117.6° and L_s 180.8° when
655 seasonal frost is still observed (Fig. 12; Suppl. Material 2). The activity ends when the
656 CO_2 disappears (Fig. 12; Suppl. Material 2) and when the surface temperature of the
657 alcove increases from 145-150K to 210-220K (Fig. 13B). CO_2 gas could play a role in
658 transporting material in the channel and on to the debris apron. Based on our
659 observations, and on comparisons with terrestrial analogues in Table 2, we propose
660 that a hyper-concentrated flow, where the fluid is not constituted by liquid water, but
661 instead by CO_2 gas, could explain this gully activity. Specifically, after falling onto the
662 floor of the alcove, the CO_2 ice should sublimate vigorously via contact with the
663 relatively hot sand previously accumulated at the foot of the alcove. Exposed to more
664 solar insolation, this sand should have a temperature significantly higher than the
665 CO_2 ice sublimation temperature producing a high gas escape rate. This initial and
666 vigorous sublimation of the CO_2 ice triggers a CO_2 gas flow mixed with sand and
667 perhaps some ice and is the process responsible for the gully activity, the
668 development of sinuosity and for the new apron deposits (Table 2). The main activity
669 occurs during the winter and not at the end of winter when temperatures are warmer,
670 because at the end of winter CO_2 ice has almost entirely disappeared from the dune
671 surface and hence there would not be sufficient CO_2 ice to drive vigorous

672 sublimation. At the end of winter, the transport is limited by the reduced availability of
673 CO_2 ice, whereas at the beginning of winter this is not the case, even if the
674 temperature difference between the CO_2 ice and the hot sand could potentially
675 produce high sublimation rate.

676 Determining exactly how a mixture of sublimating CO_2 ice and sand can produce
677 landforms similar to those produced by hyper-concentrated water flows on Earth is a
678 detailed modelling exercise beyond the scope of this study. We acknowledge that
679 important physical differences exist between the fluids of water and CO_2 gas
680 including compressibility, density and buoyancy, which would lead to significant
681 differences in behavior.

682

683 ### 4.4. Conceptual model for the development of sinuous gully channels

684 Based on our observations, we propose the following three-step conceptual
685 model for the development of sinuous gully channels (Fig. 14).

686 i) *Material accumulation at the foot of equator-facing alcove flanks (Fig. 14A).*

687 First, during Year N (section 3.3.1.2.), sand falls from equator-facing flanks estimated
688 to be at 24-26° slope in the sub-alcoves A_{4a}, A_{4b} and A_5 (Figs. 2E; 7; 5C; Suppl.
689 Material 1; 3)). The sand accumulates on the floor of the alcove during winter and
690 spring (Figs. 7; 12AE). This accumulation occurs preferentially during the middle of
691 winter and the early spring. Although for MY30 this activity is observed from early
692 winter to late spring (Fig. 12A). Around 31 800 m² or ~7% of the total area of the
693 alcove was resurfaced during MY29-33 (Fig. 7D). While no seasonal frosts were
694 observed on these slopes on HiRISE images (Fig. 12B), CRISM observations
695 indicate that CO_2 and H_2O ice cover most of the Matara Crater dunefield during mid-
696 winter, including equator-facing flanks, flat terrains, and extend to the bottom part of
697 equator-facing flanks with angles lower than 5-10° (Vincendon 2015). Seasonal ice is
698 thus probably very thin or located in the subsurface on the equator-facing flanks
699 where the activity occurs. However, sand material transport and accumulation on the
700 floor of the alcove is also observed at the end of spring (up to L_s 249.9° Fig. 12A),
701 despite the whole Matara Crater dunefield being entirely defrosted by L_s 192° (see
702 e.g., CRISM observation FRT #1C413). As a consequence, some of the observed
703 equator-facing flank material movements are very likely not related to seasonal frost.

704 This activity is never observed during summer and autumn, although the lack of
705 images at the end of spring and during summer during several years may bias our
706 interpretation. Overall, these observations support the idea that i) this activity is
707 seasonally favored, which may result from the role of temperature, ice, dust or wind
708 and ii) this activity can occur when seasonal ice is not present.

709 ii) *Seasonal frost deposition on pole-facing alcove flanks (Fig. 14B)*.

710 Second, during Year N+1, seasonal frost mainly composed of CO_2 with some H_2O is
711 observed during the cold seasons of autumn and winter on the pole-facing flanks of
712 the alcove (Figs. 12DE; 13A). The seasonal CO_2 ice deposit is several orders of
713 magnitude thicker than the H_2O ice (Fig. 13A, mm compared to µm). CO_2 is not
714 present over the whole surface of the alcove, it is mainly located on the pole-facing
715 flank of each sub-alcove A_1 to A_5 in autumn and winter between L_s 40-60° and L_s 180-
716 190° (Figs. 13A; 8AC; 5B). The maximum thickness of CO_2 frost deposit occurs at L_s
717 ~140-150° (Fig. 13A).

718 iii) *defrosting and development of channel sinuosity (Fig. 14C)*

719 Third, still during Year N+1, contemporaneously with the sudden collapse of seasonal
720 frost during the middle of winter on parts of the pole-facing flanks of sub-alcoves A_{4a}
721 to A_5, solid material is transported from the floors of the alcove to the debris apron
722 (Figs. 8; Suppl. Material 2). This timing is consistent with the retreat of the seasonal
723 frost deposits predicted by our simulations (Fig. 13). More precisely, we observed the
724 collapse of part of the slope of the alcove contemporaneously with the disappearance
725 of seasonal frost (Figs. 8; 12CDE; 13A; Suppl. Material 2). This collapse of sand
726 material on pole-facing flanks includes the seasonal CO_2 and H_2O frost present on
727 the same area (Fig. 8) incorporating them into the flow through the channel and onto
728 the apron.

729 There is a temporal correlation between the seasonal frost retreat and the
730 changes observed in the gully channel and on the apron (Figs.8; 12CDE; 13A; Suppl.
731 Material 2). The development of sinuosity in the channel is contemporaneous with the
732 sand remobilization from the floor of the sub-alcoves A_{4a}, A_{4b} and A_5 on to the debris
733 apron (Fig. 5BCD). After the sand accumulation on the floor of the sub-alcoves A_{4a} to
734 A_5, the material is evacuated toward the debris apron of the gully (Fig. 5CD).

735 Significant morphological changes of the debris apron can be observed such as an
736 elongation and increase in overall area (Figs. 11; 6EF; 5B). A process similar to
737 hyper-concentrated flows on Earth (Table 2) with an alternation of the alcove source
738 location could be responsible for the development of channel sinuosity and for the
739 new apron deposits. CO_2 gas mixed with sand, and likely some CO_2 and H_2O frost,
740 would constitute the flow from the alcove on to the debris apron. The defrosting of
741 seasonal CO_2 ice alone seems unable to cause channel and apron changes when
742 there is no material accumulation in the alcove.
743

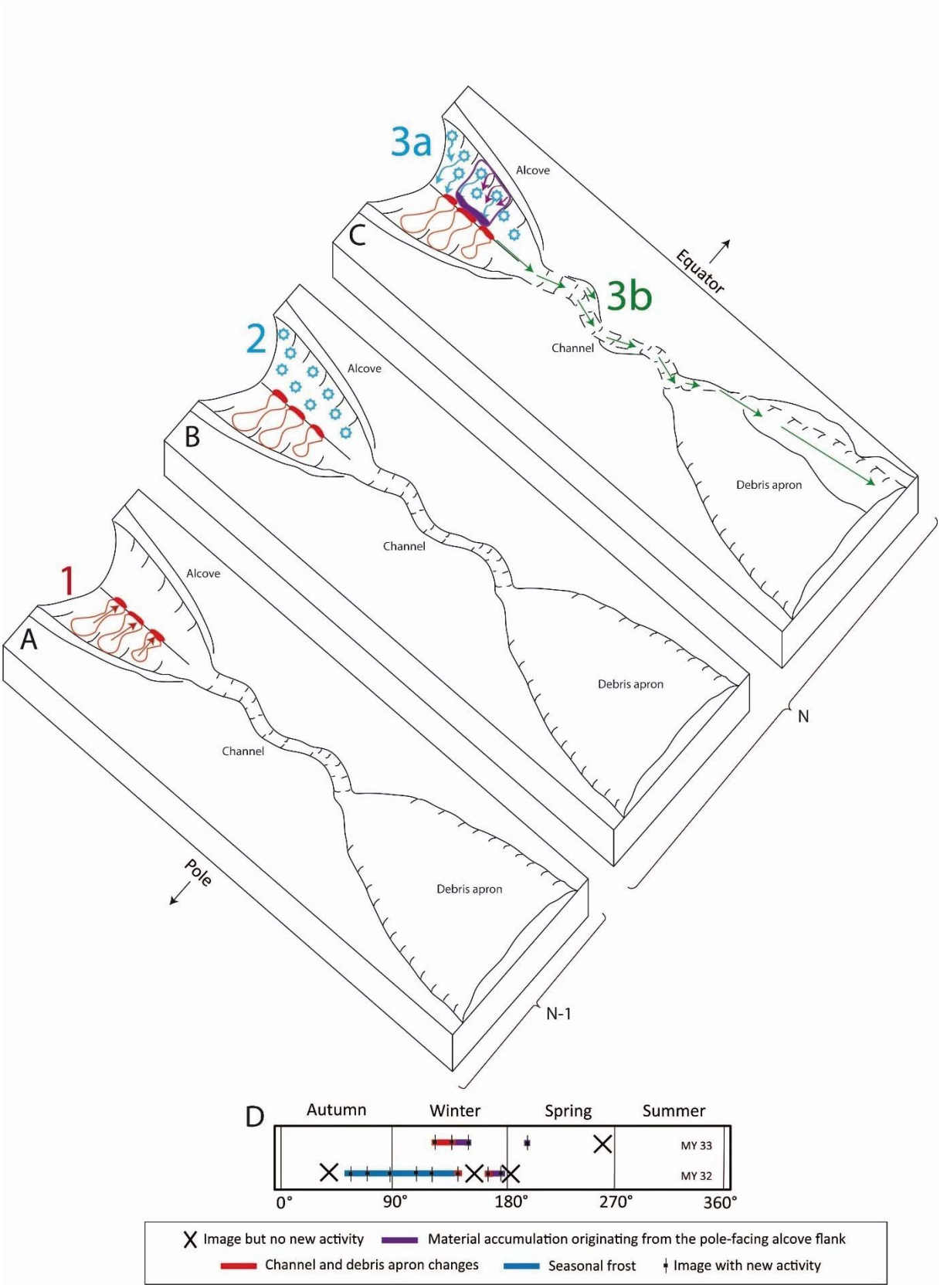

744

745 Fig. 14. A) Material accumulation on the alcove floor sourced from the equator-facing part of the
746 alcove during Year N represented by red shapes and arrows. B) Seasonal frost deposits on the pole-
747 facing flanks in autumn and winter during Year N+1, represented by blue flakes, C) Sudden defrosting

of the seasonal frost deposits, remobilization and transport of material toward the debris apron with development of channel sinuosity during Year N+1, represented by purple and green shapes and arrows, D) Timing of activity: after material accumulation in the alcove occurs in MY32, we observe development of channel sinuosity in MY33 together with deposition on the apron.

5 Conclusions

Here we describe in detail the present day development of a martian sinuous gully over 5 martian years (MY29-33). Our aim was to better understand the dynamics and the processes involved in developing gully channel sinuosity. Our observations show:

- CO_2 frost deposits during autumn and winter (L_s 40-60° to L_s 180-190°) on pole-facing alcove flanks in the gully on the Matara Crater dunefield with an estimated ice thickness of ~10 cm.

- an accumulation of sand in the alcove, takes place during winter and spring sourced by failures on the equator-facing flank. This material is later remobilized to drive changes in the channel and apron morphology.

- material transport from the alcove floors to the debris apron concurrent with channel morphology changes such as sinuosity development and new apron deposits. This activity occurs every year and often coincides with the middle of winter. It is contemporaneous with material collapse on the pole-facing alcove flank and sudden disappearance of the seasonal CO_2 frost in the collapsed zone. We hypothesize that the collapse of solid CO_2 onto the relatively warm loose sand deposits on the alcove floor mixes the materials causing vigorous sublimation and subsequent mobilization as a gas-supported flow.

- the development of channel sinuosity occurs over a timescale of 5 martian years and rates of lateral migration is on average of ~ 23 m/yr (calculated over 3 MY).

A link between CO_2 defrosting and this gully activity is consistent with its timing. We hypothesize that a flow composed of sand, CO_2 gas and ice together with the contribution of material from alternating alcove sources can explain the development of sinuous gully channels.

Acknowledgments

This study has been funded by the PNP-INSU-CNRS. Thierry G. is acknowledged for his contribution to the discussion. We thank the HiRISE team for collection of the series of monitoring images that made this study possible. SJC gratefully acknowledges the French Space Agency CNES for financial support of her HiRISE related work.

References

Allen, J.R.L., 1985. Principles of Physical sedimentology. Georges Allen and Unwin, London.

Allen, P., 1997. Earth Surface Processes, blackwell science ed.

Auld, K.S., Dixon, J.C., 2016. A classification of martian gullies from HiRISE imagery. Planet. Space Sci. 131, 88-101. http://dx.doi.org/10.1016/j.pss.2016.08.002.

Balme, M., Mangold, N., Baratoux, D., Costard, F., Gosselin, M., Masson, P., Pinet, P., Neukum, G. 2006. Orientation and distribution of recent gullies in the southern hemisphere of Mars: Observations from High Resolution Stereo Camera/ Mars Express (HRSC/MEX) and Mars Orbiter Camera/Mars Global Surveyor (MOC/MGS) data. J. Geophy. Res. (Planets), 111 (E5). http://dx.doi.org/ 10.1029/2005JE002607E5.

Bandfield, J.L., 2002. Global mineral distributions on Mars. J. Geophy. Res. Planets 107 (E6), 5042. http://dx.doi.org/10.1029/2001JE001510.

Cedillo-Flores, Y., Treiman, A.H., Lasue, J., Clifford, S.M., 2011. CO_2 gas fluidization in the initiation and formation of martian polar gullies. Geophys. Res. Lett. 38, L21202. http://dx.doi.org/10.1029/2011GL049403.

Christensen, P.R., 2003. Formation of recent martian gullies through melting of extensive water-rich snow deposits. Nature 422, 45-48. http://doi:10.1038/nature01436.

Conway, S. J., Balme M. R., 2016. A novel topographic parameterization scheme indicates that martian gullies display the signature of liquid water. Earth and Planetary Science Letters, 454, 36–45. https://doi.org/10.1016/j.epsl.2016.08.031.

807 Conway, S. J., &Balme, M. R., 2014.Decameter thick remnant glacial ice deposits on
808 Mars. Geophysical Research Letters, 41(15), 5402-5409.
809 https://doi.org/10.1002/2014GL060314.

810 Conway, S. J., Balme, M. R., Murray, J. B., Towner, M. C., Okubo, C. H., Grindrod,
811 P. M. 2011. The indication of martian gully formation processes by slope–area
812 analysis. The Geological Society, London, Special publications, 356(1), 171–201.
813 https://doi.org/10.1144/SP356.10.

814 Conway, S. J., Harrison, T. N., Soare, R. J., Britton, A. W., and Steele, L.J., 2017.
815 New slope-normalised global gully density and orientation maps for Mars. The
816 Geological Society of London, Special publications, 467.
817 https://doi.org/10.1144/SP467.3.

818 Conway, S. J., de Haas T. and Harrison, 2018. Martian gullies: a comprehensive
819 review of observations, mechanisms and insights from Earth analogues. The
820 Geological Society of London, Special publications, 467.
821 https://doi.org/10.1144/SP467.14.

822 Costard, F., Forget, F., Mangold, N., Peulvast, J.P., 2002. Formation of recent
823 Martian debris flows by melting of near-surface ground ice at high obliquity. Planet.
824 Sci. 295, 110-113. http://dx.doi.org/10.1126/science.1066698.

825 Coussot, P. and Meunier, M. 1996. Recognition, classification and mechanical
826 description of debris flows. Earth Sci. Reviews 40, 209-227. http:// doi:10.1016/0012-
827 8252(95)00065-8.

828 Di Achille, G., Silvestro, S., Ori, G.G., 2008. Defrosting processes on dark dunes:
829 new insights from HiRISE images at Noachis and Aonia Terrae, Mars. In: Planetary
830 Dunes Workshop, pp. 27-28.

831 Dickson, J., Head, J., Kreslavsky, M., 2007. Martian gullies in the southern mid-
832 latitudes of Mars: Evidence for climate-controlled formation of young fluvial features
833 based upon local and global topography. Icarus 188, 315-323.
834 http://dx.doi.org/10.1016/j.icarus.2006.11.020.

835 Diniega, S., Byrne, S., Bridges, N.T., Dundas, C.M., McEwen, A.S., 2010.
836 Seasonality of present-day martian dune-gully activity. Geology 38, 1047–1050.
837 http://dx.doi.org/10.1130/G31287.1.

838 Diniega, S., Hansen, C.J., McElwaine, J.N., Hugenholtz, C.H., Dundas, C.M.,
839 McEwen, A.S., Bourke, M.C., 2013. A new dry hypothesis for the formation of Martian
840 linear gullies. Icarus 225, 526-537. http://dx.doi.org/10.1016/j.icarus.2013.04.006.

841 Dundas, C.M., Bramson, A.M., Ojha, L., Wray, J.J., Mellon, M.T., Byrne, S., McEwen,
842 A.S., Putzig, N.E., Viola, D., Sutton, S., Clark, E., Holt, J.W. 2018. Exposed sub-
843 surface ice sheets in the Martian mid-latitudes. Sciences, 359, 199-201.
844 http://doi.org/10.1126/science.aao1619.

845 Dundas, C.M., Diniega, S., Hansen, C.J., Byrne, S., McEwen, A.S., 2012. Seasonal
846 activity and morphological changes in Martian gullies. Icarus 220, 124-143.
847 http://dx.doi.org/ 10.1016/j.icarus.2012.04.005.

848 Dundas, C.M., Diniega, S., McEwen, A.S., 2015. Long-term monitoring of martian
849 gully formation and evolution with MRO/HiRISE. Icarus 251, 244-263.
850 http://dx.doi.org/10.1016/j.icarus.2014.05.013.

851 Dundas, C.M., McEwen, A.S., Diniega, S., Byrne, S., Martinez-Alonso, S., 2010. New
852 and recent gully activity on Mars as seen by HiRISE. Geophys. Res. Lett. 37,
853 L07202. http://dx.doi.org/10.1029/2009GL041351.

854 Dundas, C. M., McEwen, A. S., Diniega, S., Hansen, C. J., Byrne, S., McElwaine, J
855 .N., 2017. The formation of gullies on Mars today. The Geological Society, London,
856 Special publications, 467. https://doi.org/10.1144/SP467.5.

857 Edwards, S.F., Liverpool, T.B., 1995. Dynamics of a Meandering River. Phys. Rev.
858 Lett. 75, 3016. https://doi.org/10.1103/PhysRevLett.75.3016.

859 Fenton, L. K., & Hayward, R. K., 2010. Southern high latitude dune fields on Mars:
860 Morphology, aeolian inactivity, and climate change. Geomorphology, 121(1-2), 98-
861 121. https://doi.org/10.1016/j.geomorph.2009.11.006.

862 Forget, F., Hourdin, F., Fournier, R., Hourdin, C., Talagrand, O., Collins, M., Lewis, S.
863 R., Read, P. L., Huot, J. P., 1999. Improved general circulation models of the martian

atmosphere from the surface to above 80 km. Journal of Geophysical Research Planets, 104(E10), 24,155–24,175. https://doi.org/10.1029/1999JE001025.

Forget, G., Ferron, B., Mercier, H., 2008. Combining argo profiles with a general circulation model in the north atlantic. Part 1: Estimation of hydrographic and circulation anomalies from synthetic profiles, over a year. Ocean Modelling, 20(1), 1–16. https://doi.org/10.1016/j.ocemod.2007.06.001.

Gaidos, E.J. 2001. Cryovolcanism and the Recent Flow of Liquid Water on Mars. Icarus 153, 218-223. http://doi:10.1006/icar.2001.6649.

Gardin, E., Allemand, P., Quantin, C., Thollot, P., 2010. Defrosting, dark flow features, and dune activity on Mars: Example in Russell crater. J. Geophys. Res. 115, 1–9. http://dx.doi.org/10.1029/2009JE003515.

Hauber, E., Reiss, D., Ulrich, M., Preusker, F., Trauthan, F., 2011. Landscape evolution in Martian mid-latitude regions: insights from analogous periglacial landforms in Svalbard. The Geological Society of London, Special Publications, 356. https://doi.org/10.1144/SP356.7.

Hansen, C.J., Bourke, M., Bridges, N.T., Byrne, S., Colon, C., Diniega, S., Dundas, C., Herkenhoff, K., McEwen, A., Mellon, M., Portyankina, G., Thomas, N.2011. Seasonal erosion and restoration of Mars' northern polar dunes. Science 331, 575–578. http://dx.doi.org/10.1126/science.1197636.

Harrison, T.N., Osinski, G.R., Tornabene, L.L., Jones, E., 2015. Global documentation of gullies with the Mars Reconnaissance Orbiter Context Camera and implications for their formation. Icarus 252, 236–254. http://dx.doi.org/10.1016/j.icarus.2015.01.022.

Hartmann, W. K., 2001. Martian seeps and their relation to youthful geothermal activity. Space Sci. Reviews 96, 405-410. http://doi:10.1007/978-94-017-1035-0_15.

Hayward, R.K., Fenton, L.K., Titus, T.N., 2014. Mars Global Digital Dune Database (MGD3): Global dune distribution and wind pattern observations. Icarus 230, 38–46. http://dx.doi.org/10.1016/j.icarus.2013.04.011.

892 Hecht, M. H. (2002), Metastability of liquid water on mars, Icarus, 156(2), 373–386.
893 https://doi.org/10.1006/icar.2001.6794.

894 Heldmann, J. H., Mellon, M. T. 2004. Observations of martians gullies and
895 constraints on potential formation mechanisms. Icarus 168, 285-304.
896 http://dx.doi.org/10.1016/j.icarus.2003.11.024.

897 Heldmann, J. L., Toon, O. B., Pollard, W. H., Mellon, M. T., Pitlick, J., McKay, C. P.,
898 and Andersen, D. T. 2005. Formation of Martian gullies by the action of liquid water
899 flowing under current Martian environmental conditions. J. Geophys. Res. 110,
900 E05004. http://doi:10.1029/2004JE002261.

901 Herkenhoff, K.E., Vasavada, A.R., 1999. Dark material in the polar layered deposits
902 and dunes on Mars. J. Geophys. Res. 104 (E7), 16487-16500.
903 http://dx.doi.org/10.1029/1998JE000589.

904 Hickin, E., 1974. The development of meanders in natural river-channel, American
905 Journal of Science, 274, 414–442. https://doi.org/10.2475/ajs.274.4.414.

906 Hoffman, N., 2002. Active Polar gullies on Mars and the Role of Carbon Dioxide.
907 Astrobiology 2, 313-323. http://doi:10.1089/153110702762027899.

908 Hugenholtz, C.H. 2008. Frosted granular flow: A new hypothesis for mass wasting in
909 martian gullies. Icarus 197, 65-72. http://dx.doi.org/10.1016/j.icarus.2008.04.010.

910 Ishii, T., Sasaki, S., 2004.Formation of recent martian gullies by avalanches of CO_2
911 frost. Lunar Planet.Sci. 35. Abstract 1556.

912 Johnson, A., Rodine, J., 1984. Debris flow, Slope instability, pp. 257–361.

913 Jouannic, G., Gargani, J., Conway, S.J., Costard, F., Balme, M.R., Patel, M.R.,
914 Massé, M., Marmo, C., Jomelli, V., Ori, G.G., 2015. Laboratory simulation of debris
915 flows over sand dunes: Insights into gully-formation (Mars). Geomorphology 231,
916 101–115. http://dx.doi.org/10.1016/j.geomorph.2014.12.007.

917 Jouannic, G., Gargani, J., Costard, F., Massé, M., Bourgeois, O., Carter, J., Schmidt,
918 F., Marmo, C., Ori., G., Nachon, M., Pasquon, K., 2018. Morphological
919 characterization of landsforms produced by springtime seasonal activity on Russell

dune (Mars), The Geological Society, London, Special publications. https://doi.org/10.1144/SP467.16.

Jouannic, G., Gargani, J., Costard, F., Ori, G.G., Marmo, C., Schmidt, F., Lucas, A., 2012. Morphological and mechanical characterization of gullies in a periglacial environment: The case of the Russell crater dune Mars. Planet.Space. Sci. 71, 38-54. http://dx.doi.org/10.1016/j.pss.2012.07.005.

Kereszturi, A., Möhlmann, D., Berczi, S., Ganti, T., Kuti, A., Sik, A., Horvath, A., 2009. Recent rheologic processes on dark polar dunes of Mars: Driven by interfacial water? Icarus 201, 492-503. http://dx.doi.org/10.1016/j.icarus.2009.01.014.

Kieffer, H. H., 2000. Annual punctuated CO_2 slab-ice and jets on Mars. 2nd Int. Conf. Mars Polar Sci. Abstract 4095.

Kieffer, H.H., 2007. Cold jets in the Martina polar caps, J. Geophys. Res. 112. E08005. http://dx.doi.org/10.1029/2006JE002816.

Kieffer, H.H., Christensen, P.R., Titus, T.N., 2006. CO_2 jets formed by sublimation beneath translucent slab ice in Mars seasonal south polar ice cap. Nature 442, 793-796. http://dx.doi.org/10.1038/nature04945.

Knauth, J.P., Burt, D.M., 2002. Eutectic brines on Mars: Origin and possible relation to young seepage features. Icarus 158, 267-271. http://dx.doi.org/10.1006/icar.2002.6866.

Kossacki, K. J., Markiewicz, W. J., 2004. Seasonal melting of surface water ice condensing in martian gullies. Icarus 171, 272-283. https://doi.org/10.1016/j.icarus.2004.05.018.

Lee, P., Cockell, C. S., Marinova, M. M., McKay C. P., Rice, J. W., 2001. Snow and Ice Melt Flow Features on Devon Island, Nunavut, Arctic Canada as Possible Analogs for Recent Slope Flow Features on Mars. Lunar and Planetary Science Conference 32 (abstract 1809).

Lemmon, M. T., Wolff, M. J., Bell, J. F., Smith, M. D., Cantor, B. A., Smith, P. H. 2015. Dust aerosol, clouds, and the atmospheric optical depth record over 5 mars

948 years of the mars exploration rover mission. Icarus, 251, 96–111.
949 https://doi.org/10.1016/j.icarus.2014.03.029.

950 Leopold, L. B., and Wolman, M. G., 1960. River meanders, Geological Society of
951 America Bulletin, 71(6), 769–793. https://doi.org/10.1130/0016-
952 7606(1960)71[769:RM]2.0.CO;2.

953 Malin, M.C., Edgett, K.S., Posiolova, L.V., McColley, S.M., NoeDobrea, E.Z., 2006.
954 Present-Day Impact Cratering Rate and Contemporary Gully Activity on
955 Mars.Science 314, 1573. http://doi10.1126/science.1135156.

956 Malin, M.C., Edgett, K.S., 2000. Evidence for recent groundwater seepage and
957 surface runoff on Mars. Sciences 288, 2330-2335.
958 http://dx.doi.org/10.1126/science.288.5475.233.

959 Mangold, N., Costard, F. Forget. F., 2003. Debris flows over sand dunes on Mars:
960 Evidence for liquid water, J. Geophys. Res., 108 (E4), 5027.
961 http://dx.doi.org/10.1029/2002JE001958.

962 Mangold, N., Mangeney, A., Migeon, V. Ansan, V., Lucas, A., Baratoux, D., Bouchut,
963 F., 2010. Sinuous gullies on Mars: Frequency, distribution, and implications for flow
964 properties. J. Geophys. Res. 115, E11001. http://dx.doi.org/10.1029/2009JE003540.

965 Massé, M., Conway, S.J., Gargani, J., Patel, M.R., Pasquon, K., McEwen, A., Carpy,
966 S., Chevrier, V., Balme, M., Ojha, L., Vincendon, M., Poulet, F., Costard, F.,
967 Jouannic, G., 2016. Transport processes induced by metastable boiling water under
968 Martian surface conditions. Nature geosc. 9, 425-428. http://doi:10.1038/NGEO2706.

969 McEwen, A. S. et al., 2010. The High Resolution Imaging Science Experiment
970 (HiRISE) during MRO's Primary Science Phase (PSP). Icarus 205, 2-37.
971 http://dx.doi.org/doi:10.1016/j.icarus.2009.04.023.

972 McEwen, A. S., et al. (2007), Mars Reconnaissance Orbiter's High Resolution
973 Imaging Science Experiment (HiRISE), Journal of Geophysical Research: Planets,
974 112(E5). https://doi.org/10.1029/2005JE002605.

975 Mellon, M.T., Feldman, W.C., Prettyman, T.H., 2004. The presence and stability of
976 ground ice in the southern hemisphere of Mars. Icarus 169, 324–340.
977 https://doi.org/10.1016/j.icarus.2003.10.022.

978 Mellon, M.T., Philips, R.J., 2001. Recent gullies on Mars and the source of liquid
979 water. J.Geophys.Res.106 (E10) 23165-23179. http://doi:10.1029/2000JE001424.

980 Miyamoto, H., Dohm, J. M., Baker, V. R., Beyer, R. A., Bourke, M., 2004. Dynamics
981 of unusual debris flows on martian sand dunes, Geophysical Research Letters,
982 31(13). https://doi.org/10.1029/2004GL020313.

983 Murchie, S. L., et al. 2004, CRISM (Compact Reconnaissance Imaging Spectrometer
984 for Mars) on MRO (Mars Reconnaissance Orbiter), Instruments, Science, and
985 Methods for Geospace and Planetary Remote Sensing, vol. 5660, pp. 66–78,
986 International Society for Optics and Photonics. http://doi.org/10.1117/12.578976.

987 Musselwhite, D.S., Swindle, T.D., Lunine, J.I., 2001. Liquid CO_2 breakout and the
988 formation of recent small gullies on Mars. Geophys. Res. Lett. 28, 1283-1285.
989 http://doi:10.1029/2000GL012496.

990 Ojha, L., Wilhelm, M. B., Murchie, S. L., McEwen, A. S., Wray, J. J., Hanley, J.,
991 Massé, M., and Chojnacki, M., 2015. Spectral evidence for hydrated salts in recurring
992 slope lineae on Mars, Nature Geoscience, 8(11), 829–
993 832. http://dx.doi.org/10.1038/ngeo2546.

994 Paige, D.A., Keegan, K.D., 1994. Thermal and albedo mapping of the polar regions
995 of Mars using Viking thermal mapper observations: 2. South polar region. J.
996 Geophys. Res. 99 (E12), 25993-2601. http://dx.doi.org/10.1029/93JE03429.

997 Pasquon , K., Gargani, J., Massé, M., Conway, S .J., 2016. Present-day formation
998 and seasonal evolution of linear dune gullies on Mars. Icarus 274, 195-210.
999 http://dx.doi.org/10.1016/j.icarus.2016.03.024.

1000 Pasquon, K., Gargani, J., Nachon, M., Conway, S. J., Massé, M., Jouannic, G.,
1001 Balme, M. R., Costard, F., Vincendon, M., 2018. Are different martian gully
1002 morphologies due to different processes on the kaiser dune field ? The Geological
1003 Society of London, Special publication, 467. https://doi.org/10.1144/SP467.13.

1004 Pierson, T. C., 2005. Hyperconcentrated flow—transitional process between water
1005 flow and debris flow. Debris-flow hazards and related phenomena, Springer, 159-
1006 202.

1007 Pierson, T. C., 1981. Dominant particle support mechanisms in debris flows at
1008 mtthomas, new zealand, and implications for flow mobility. Sedimentology, 28(1), 49–
1009 60. https://doi.org/10.1111/j.1365-3091.1981.tb01662.x.

1010 Pilorget, C., Forget, F., 2015. Formation of gullies on Mars by debris flows triggered
1011 by CO_2 sublimation. Nature Geosc. 9, 65-69. http://dx.doi.org/10.1038/NGEO2619.

1012 Piqueux, S., Byrne, S., Richardson, M., 2003. Sublimation of Mars southern seasonal
1013 CO_2 ice cap and the formation of spiders. J. Geophys. Res. 108 (E8) 5084.
1014 http://dx.doi.org/10.1029/2002JE002007.

1015 Piqueux, S., Christensen, P.R., 2008. North and south sub-ice gas flow and venting
1016 of the seasonal caps of Mars: A major geomorphological agent. J. Geophy. Res.
1017 Planets 113 (E6). http://dx.doi.org/10.1029/2007JE003009.

1018 Raack, J., Reiss, D., Appéré, T., Vincendon, M., Ruesch, O., Hiesinger, H., 2015.
1019 Present-day seasonal gully activity in a south polar pit (Sisyphi Cavi) on Mars. Icarus
1020 251, 226-243. http://dx.doi.org/10.1016/j.icarus.2014.03.040.

1021 Reiss, D., Jaumann, R., 2003. Recent debris flows on Mars: Seasonal observations
1022 of the Russell Crater dunefield. Geophys. Res. Lett. 30 (6):060000–1.
1023 http://dx.doi.org/10.1029/2002GL016704.

1024 Reiss, D., Erkeling, G., Bauch, K.E. and Hiesinger, H. 2010. Evidence for present day
1025 Gully on the Russell crater dunefield, Mars. Geophys. Res. Lett. 37, L06203.
1026 http://dx.doi.org/10.1029/20090421192.

1027 Schorghofer, N., Edgett, K.S., 2006. Seasonal surface frost at Low latitudes on Mars.
1028 Icarus 180, 321–334. http://dx.doi.org/10.1016/j.icarus.2005.08.022.

1029 Shinbrot, T., Duong, N.H., Kwan, L., Alvarez, M.M., 2004. Dry granular flows can
1030 generate surface features resembling those seen in martian gullies. Proc.Natl. Acad.
1031 Sci.101, 8542-8546. http://doi: 10.1073/pnas.0308251101.

1032 Smith, D. E., Zuber, M. T., Neumann, G. A. 2001. Seasonal Variations of Snow
1033 Depth on Mars. Science, 294, 2141–2146.
1034 http://dx.doi.org/10.1126/science.1066556.

1035 Spiga, A., Forget, F., 2008. Fast and accurate estimation of solar irradiance on
1036 martian slopes. Geophysical Research Letters, 35(15).
1037 https://doi.org/10.1029/2008GL034956.

1038 Sylvest, M.E., Conway, S.J., Patel, M.R., Dixon, J., Barnes, A., 2015. Laboratory
1039 observations of mass wasting triggered by sublimation of condensed CO_2 frost under
1040 Martian conditions. Lunar Planet.Sci. 46. Abstract 2667.

1041 Sylvest, M. E., Dixon, J.C., Conway, S.J., Patel, M.R., McElwaine, J.N., Hagermann,
1042 A., Barnes, A, 2018. CO_2 sublimation in Martian gullies: laboratory experiments at
1043 varied slope angle and regolith grain sizes. The Geological Society, London, Special
1044 publications, 467. https://doi.org/10.1144/SP467.11.

1045 Thomas, P., 1982. Present wind activity on Mars - Relation to large latitudinal zoned
1046 sediment deposits. J. Geophys. Res. 87, 9999-10008.
1047 http://dx.doi.org/10.1029/JB087iB12p09999.

1048 Treiman, A.H., 2003. Geologic setting of martian gullies: implications for their origins.
1049 J. Geophy. Res. 108 (E4), 8031. http://doi:10.1029/2002JE001900.

1050 Vincendon, M., Mustard, J., Forget, F., Kreslavsky, M., Spiga, A., Murchie, S.,
1051 Bibring, J-P., 2010a. Near-tropical subsurface ice on Mars. Geophys. Res. Lett. 37,
1052 L01202. http://dx.doi.org/10.1029/2009GL041426, 2010.

1053 Vincendon, M., Forget, F., Mustard, J., 2010b. Water ice at low to mid-latitudes on
1054 Mars. J. Geophys. Res. 115, E10001. http://dx.doi.org/10.1029/2010JE003584,
1055 2010.

1056 Vincendon, M. 2015. Identification of Mars gully activity types associated with ice
1057 composition. J. Geophys. Res. Planets, 120.
1058 http://dx.doi.org/doi:10.1002/2015JE004909.

1059 Védie, E., Costard, F., Font, M., and Lagarde, J., 2008. Laboratory simulations of
1060 martian gullies on sand dunes, Geophysical Research Letters, 35(21).
1061 https://doi.org/10.1029/2008GL035638.

1062 Williams, G.P. 1986. River meanders and channel size. Journal of Hydrology, 88,
1063 147-164. https://doi.org/10.1016/0022-1694(86)90202-7.

1064 Williams, K.E., Toon, O.B., Heldmann, J.L., Mellon, M.T., 2009. Ancient melting of
1065 mid-latitude snowpacks on Mars as a water source for gullies. Icarus 200, 418-425.
1066 http://dx.doi.org/10.1016/j.icarus.2008.12.013.

1067 Ward, A. W., Doyle, K. B., 1983. Speculation on Martian north polar wind circulation
1068 and the resultant orientations of polar sand dunes. Icarus 55, 420-431.
1069 http://dx.doi.org/10.1016/0019-1035(83)90112-4.

Supplementary material

Sub-alcove	Pole facing slope (°)	Equator facing slope (°)
A1	22.4	19.5
A2	22.5	18.6
A3	23.8	21.0
A4a	24.2	25.0
A4b	22.6	25.6
A5	23.8	26.3
average	**23.2**	**22.7**

Suppl. Material 1. Slopes of the sub-alcoves.

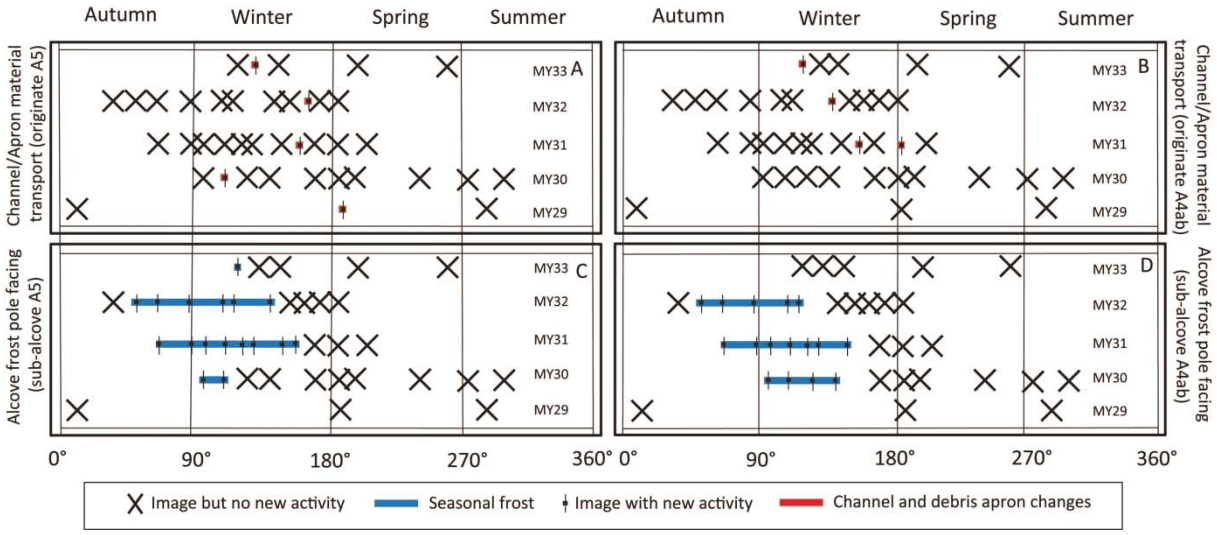

Suppl. Material. 2. A) Timing of presence of seasonal frost for sub-alcove A_5 on pole facing slopes. B) Timing of presence of seasonal frost for sub-alcoves A_{4a}, A_{4b} on pole facing slopes, C) Timing of activity for material transport from the sub-alcove A_5 to the apron synchronous with sinuosity development, D) Timing of activity for material transport from the sub-alcoves A_{4a}, A_{4b} to the apron synchronous with sinuosity development. Each line represents one martian year and each cross (or vertical line) is a HiRISE image.

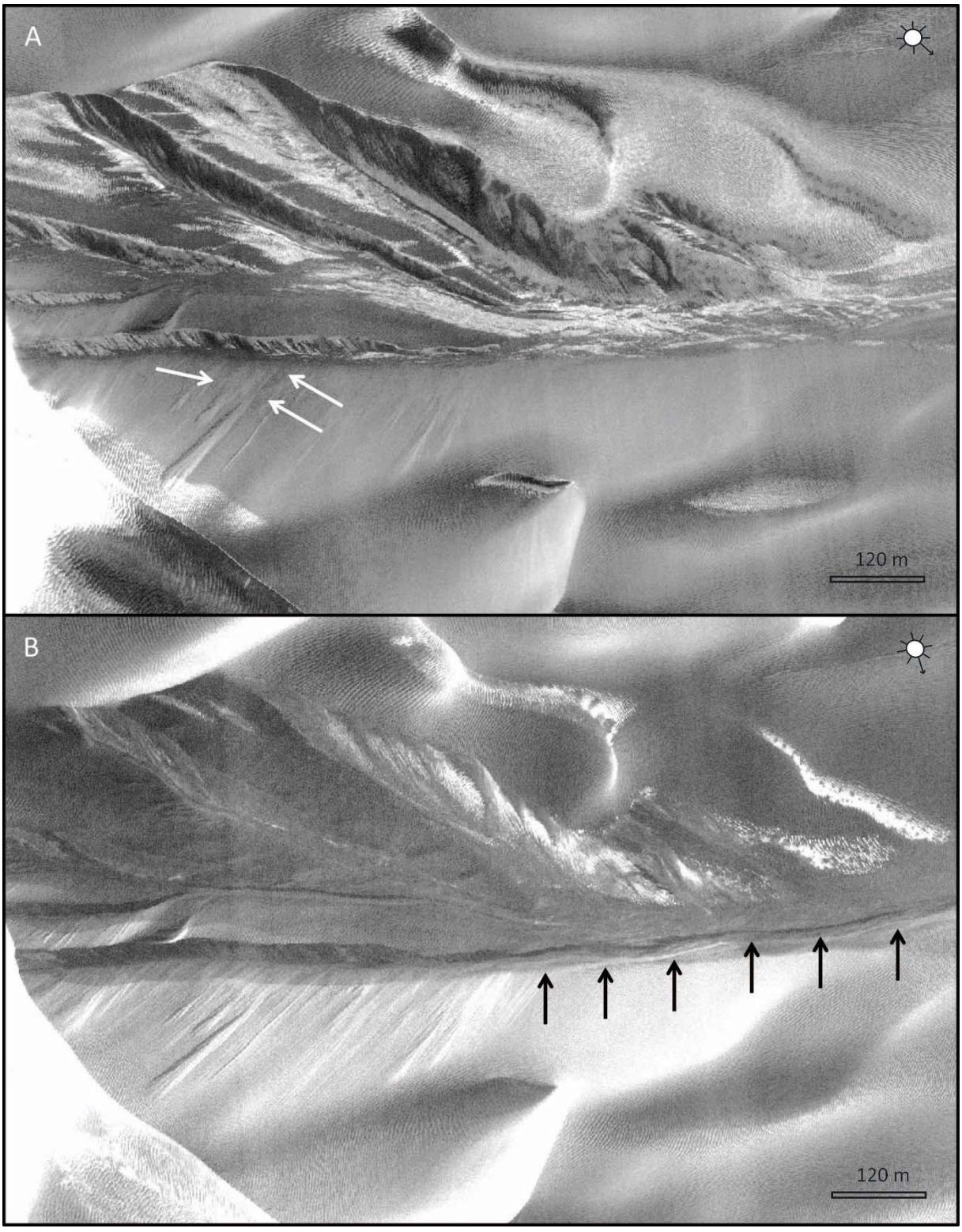

Suppl. Material 3. Alcove activity: A) material accumulation on equator facing slope (white arrow) (HiRISE image: ESP_027838_1300, Ls 134.4°), B) transport of material accumulated on the equator facing slope toward the debris apron. Erosion of a channel on the floor of the alcove (black arrows) (HiRISE image: ESP_028405_1300, Ls 156.7°).